Chemical Science

ROYAL SOCIETY OF CHEMISTRY

REVIEW

View Article Online
View Journal | View Issue

Check for updates

Cite this: *Chem. Sci.*, 2023, **14**, 12850

Optimization strategies of high-entropy alloys for electrocatalytic applications

Liyuan Xiao, Zhenlu Wang * and Jingqi Guan *

High-entropy alloys (HEAs) are expected to become one of the most promising functional materials in the field of electrocatalysis due to their site-occupancy disorder and lattice order. The chemical complexity and component tunability make it possible for them to obtain a nearly continuous distribution of adsorption energy curve, which means that the optimal adsorption strength and maximum activity can be obtained by a multi-alloying strategy. In the last decade, a great deal of research has been performed on the synthesis, element selection and catalytic applications of HEAs. In this review, we focus on the analysis and summary of the advantages, design ideas and optimization strategies of HEAs in electrocatalysis. Combined with experiments and theories, the advantages of high activity and high stability of HEAs are explored in depth. According to the classification of catalytic reactions, how to design high-performance HEA catalysts is proposed. More importantly, efficient strategies for optimizing HEA catalysts are provided, including element regulation, defect regulation and strain engineering. Finally, we point out the challenges that HEAs will face in the future, and put forward some personal proposals. This work provides a deep understanding and important reference for electrocatalytic applications of HEAs.

Received 20th September 2023
Accepted 19th October 2023

DOI: 10.1039/d3sc04962k

rsc.li/chemical-science

Open Access Article. Published on 19 ottobre 2023. Downloaded on 01/06/2026 19:16:00.
This article is licensed under a Creative Commons Attribution-NonCommercial 3.0 Unported Licence.

1. Introduction

With the continuous development of civilization, there is growing demand for energy. To solve the problem of environmental pollution and energy shortage, people have turned to renewable energy sources such as solar energy, wind energy, and water energy in recent years, reducing the dependence on fossil energy.[1] The excess electricity generated by clean energy can be used to convert water and carbon dioxide into fuels such as hydrogen, formic acid, and methanol, which are then released through electrochemical devices such as fuel cells.[2] In the conversion process of electrical energy and chemical energy, appropriate catalysts are needed to accelerate the electrochemical reactions, thereby improving the energy efficiency. Hydrogen production by electrolysis of water is one of the ideal ways to alleviate the current energy and environmental problems, which involve the hydrogen evolution reaction (HER) and oxygen evolution reaction (OER). For the HER, Pt-group noble metals have ideal d-electron structures and are recognized as high-performance electrocatalysts.[3,4] Compared with the HER, the OER is a more complex $4e^-$ transfer process, which requires a higher overpotential and is a bottleneck restricting the development of hydrogen production technology.[5,6] The OER includes multi-step adsorption and desorption processes, and it is necessary to simultaneously improve the conductivity of the catalyst and increase the active adsorption sites to ensure that the electron and proton transport is not limited.[7] A fuel cell is a power generation device that converts chemical energy in fuels and oxidizers into electrical energy through redox reactions.[8] It has the characteristics of high energy conversion efficiency and being clean and non-polluting.[9] The oxygen reduction reaction (ORR) involves complex four-electron and four-proton transfer processes, and its slow kinetics is the main obstacle for the practical application of fuel cells.[10] As an effective way to convert CO_2 into high value-added chemicals, the electrocatalytic carbon dioxide reduction reaction (CO_2RR) is one of the important means to slow down the greenhouse effect and achieve the goal of carbon peaking and carbon neutralization.[11] At present, copper-based materials are still the only heterogeneous electrocatalysts that can selectively electrocatalyze the reduction of CO_2 to multi-carbon products.

Up to now, a large number of non-noble metal catalysts with high activity, high stability and low cost have emerged in the field of electrocatalysis. Among them, high-entropy alloys (HEAs) are composed of five or more equiatomic or near-equiatomic components, forming a simple solid solution phase.[12] Different from traditional alloys, multi-component HEAs are the result of the interaction of multiple principal elements, rather than the unique properties of a single element, with the structural characteristics of disordered occupation and ordered lattice.[13] High-entropy alloying has been widely used in the design of electrocatalysts because of rich elemental composition, adjustable electronic structure, and unique physical and chemical properties (Scheme 1). In recent years, HEAs have been widely reported in the HER,[14] OER,[15] ORR[16] and

Institute of Physical Chemistry, College of Chemistry, Jilin University, Changchun 130021, PR China. E-mail: wzl@jlu.edu.cn; guanjq@jlu.edu.cn

© 2023 The Author(s). Published by the Royal Society of Chemistry

Open Access Article. Published on 19 ottobre 2023. Downloaded on 01/06/2026 19:16:00.
This article is licensed under a Creative Commons Attribution-NonCommercial 3.0 Unported Licence.

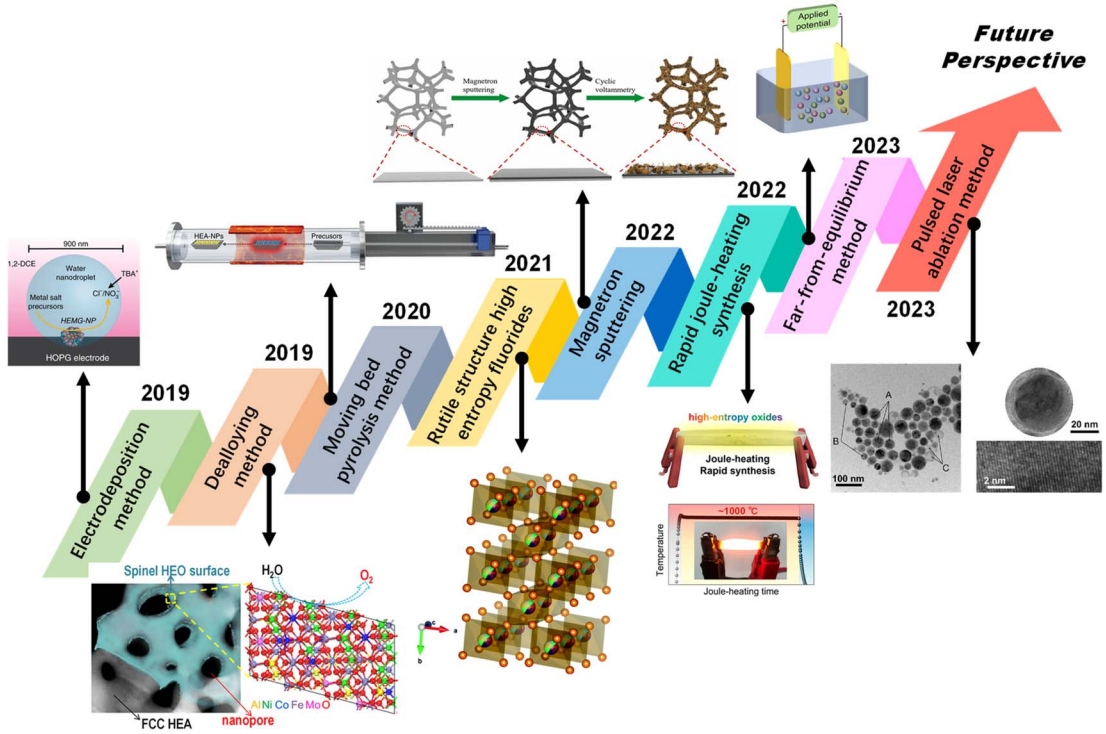

Scheme 1 Recent advances in HEAs for electrocatalysis. Reproduced with permission.[20] Copyright 2019, Springer Nature. Reproduced with permission.[21] Copyright 2021, Wiley-VCH. Reproduced with permission.[22] Copyright 2019, American Chemical Society. Reproduced with permission.[23] Copyright 2021, Royal Society of Chemistry. Reproduced with permission.[24] Copyright 2022, Elsevier Ltd. Reproduced with permission.[25] Copyright 2022, American Chemical Society. Reproduced with permission.[26] Copyright 2023, Elsevier Ltd. Reproduced with permission.[27] Copyright 2023, Elsevier Ltd.

CO_2RR.[17] On the one hand, high-entropy alloying can improve the utilization of precious metals, regulate the coordination environment and local electronic structure of precious metal atoms, and thus adjust the adsorption energy of intermediates. Xia *et al.* prepared FeCoNiRhPt HEA-NPs with an average particle size of 2 nm, which can withstand ultra-high atomic utilization.[18] X-ray absorption near-edge structure (XANES) showed that the electron density is transferred from adjacent atoms to Pt and Rh atoms. The Fermi level of Pt reduces after getting the charge, thus optimizing the hydrogen adsorption free energy. At a low overpotential, hydrogen ions are mainly adsorbed on the Rh site, and Pt becomes the main active site of the HER as the reaction begins. This work improves the atomic utilization of precious metal Pt and reveals the catalytic mechanism of multi-site cooperative work in precious metal high-entropy catalysts. Furthermore, the interaction of different elements in the high-entropy catalyst provides a unique surface binding site to achieve selective adsorption of different reactants and intermediates, which effectively promotes the rate-determining step. Nellaiappan *et al.* prepared an AuAgPtPdCu HEA for the CO_2RR,[19] over which the main products are CO, CH_4, C_2H_4 and H_2, and the total Faraday efficiency (FE) of the gaseous products at low potentials is 100%. DFT calculations showed that the random distribution of elements in the HEA promotes the formation of abundant active centers on the surface, which optimizes the adsorption energy of reaction intermediates. In addition, high-entropy alloying regulates the electronic interaction of the metal–oxygen bond. The hysteresis diffusion effect can improve the dynamic stability of the catalyst and enable it to achieve effective expression of active sites in harsh environments such as strong corrosion and high potential.

Here, we summarize the strategies for regulating HEAs to improve electrocatalytic performances, providing guidance for future research. Firstly, the structure, core effect and preparation method of HEAs are introduced, the applicable conditions of each synthesis method are analyzed, and the advanced characterization methods for revealing HEAs are introduced. Secondly, the advantages of HEAs for electrocatalysis are introduced from both experimental and theoretical aspects, and how to design HEAs according to different reaction systems is analyzed. More importantly, on the basis of the previous literature,[28,29] we summarize several strategies for regulating HEAs to improve their catalytic activity through in-depth analysis, including element regulation, defect regulation and strain engineering. Finally, the challenges faced by high-entropy catalysts in electrocatalysis are proposed, and the prospects of their future development are discussed.

2. Properties of HEAs

2.1. Definition

The definition of HEAs can be divided into two types, one based on composition and the other based on entropy. In 2004, Yeh

Open Access Article. Published on 19 ottobre 2023. Downloaded on 01/06/2026 19:16:00.
This article is licensed under a Creative Commons Attribution-NonCommercial 3.0 Unported Licence.

et al. and Cantor *et al.* proposed the concepts of HEAs and equiatomic multi-component alloys, respectively.[30,31] High entropy alloys are composed of five or more main elements, and the atomic fraction of each main element is 5–35%. In addition, the definition of HEAs based on entropy is related to the configuration entropy of the alloy, and the entropy value is decisive in the stability of the alloy structure (Fig. 1a).[32] With the deepening of the concept, the confusion degree of atomic entropy has become the dominant factor in defining the concept. In the experiment, it was found that the ternary and quaternary alloys with an equal molar ratio or near equal molar ratio tend to form a simple solid solution phase with excellent comprehensive properties, and thereby they are also defined as HEAs. Traditional alloy development is mostly located at the corner of the phase diagram,[33] and the larger space in the middle part is often neglected (Fig. 1b). The material development of high entropy concept is to use the middle space for design and development.

2.2. Phase structure

HEAs can be divided into FCC-type (face-centered cubic structure),[34] BCC-type (body-centered cubic structure),[35] HCP-type (hexagonal close-packed structure),[36] amorphous type and intermetallic compound type.[37,38] Different atoms randomly occupy the lattice position to form a simple solid solution (Fig. 1c).[32] At present, FCC-type HEAs are the most widely studied, such as FeCoNiCrMn,[39,40] PtPdRhRuCe,[41] RuRhCoNiIr[42] and TiZrHfNbTa.[43] The FCC structure has good plasticity, but the strength is insufficient. It is worth mentioning that HEAs with FCC structure usually exhibit excellent electrocatalytic performance. Wang *et al.* prepared a powdered FCC phase $Fe_{0.5}CoNiCuZn_x$ HEA for the OER, which exhibited an overpotential of 340 mV at 10 mA cm^{-2}.[44] BCC structure (such as CrMnFeNi) has high strength and brittleness. Furthermore, it has excellent electrical conductivity and optimized electronic structure, which is superior to the FCC structure counterpart in the OER and HER.[45] The HCP structure (such as IrOsReRhRu) is less reported in electrocatalysis.

2.3. Core effects

Different from traditional alloys, HEAs have many components and complex structures, which affect the microstructure properties. HEAs have four unique effects: (1) high entropy effect in thermodynamics, (2) slow diffusion effect in dynamics, (3) structural lattice distortion effect, and (4) cocktail effect on performance. Among them, the first three effects are the assumptions based on the previously published data, while the cocktail effect is a separate characterization of HEAs, which does not need to be proved.

2.3.1. High entropy effect. The high entropy effect is a hallmark concept of HEAs, that is, five or more elements are uniformly mixed with a nearly equal molar ratio, which makes the system more inclined to form an ideal entropy solid solution, rather than fusion entropy of pure metals (Fig. 1d).[46]

2.3.2. Slow diffusion effect. The slow diffusion effect refers to the slow atomic diffusion rate and phase transformation kinetics of HEAs. The diffusion rate of atoms has a strong relationship with the grain size of the material. When the alloy is composed of nanocrystals, the transformation occurs very quickly. Only under the condition of large grains is the diffusion rate of atoms consistent with the hysteresis diffusion effect.

2.3.3. Lattice distortion effect. The lattice distortion effect refers to the phenomenon that the bond length and bond angle between adjacent atoms in the crystal structure are distorted.[47] The displacement of each lattice site depends on the atoms occupying the site and the type of atoms in the local

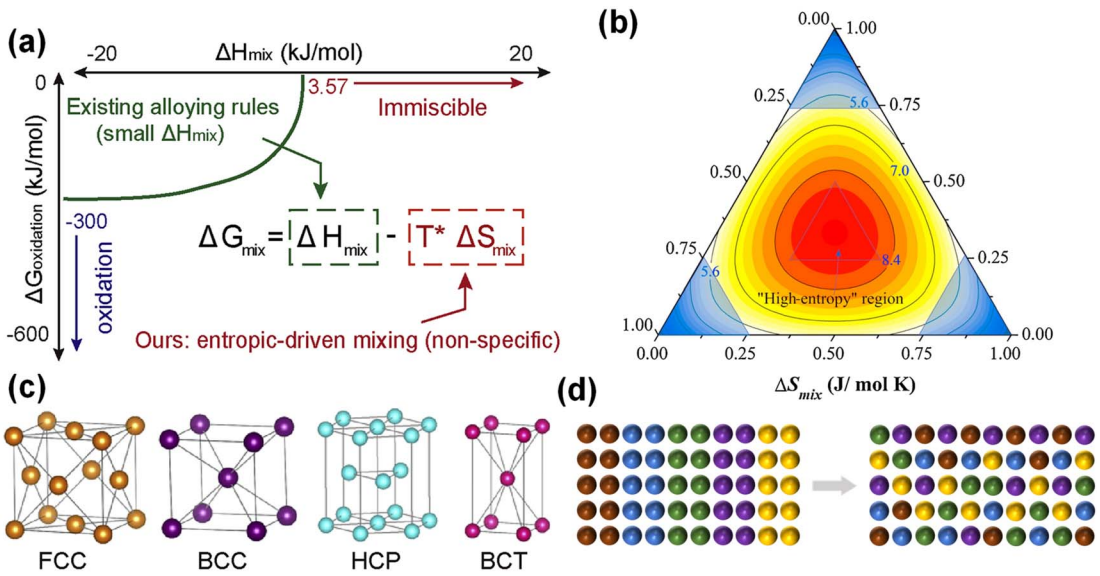

Fig. 1 (a) Enabling more alloy choices based on the entropic contribution ($-T\Delta S_{mix}$). Reproduced with permission.[32] Copyright 2021, Elsevier Ltd. (b) Different spaces of traditional alloy and high entropy alloy. Reproduced with permission.[33] Copyright 2016, Elsevier Ltd. (c) HEAs structure model. Reproduced with permission.[32] Copyright 2021, Elsevier Ltd. (d) High entropy effect.

© 2023 The Author(s). Published by the Royal Society of Chemistry

Open Access Article. Published on 19 ottobre 2023. Downloaded on 01/06/2026 19:16:00.
This article is licensed under a Creative Commons Attribution-NonCommercial 3.0 Unported Licence.

environment.[48] This effect causes inhomogeneity in the same layer of atomic planes, resulting in obvious Bragg scattering of X-rays on uneven crystal planes, thereby weakening and broadening the XRD peaks of HEAs.

2.3.4. Cocktail effect. The cocktail effect of HEAs refers to a synergistic effect caused by the interaction between adjacent elements, that is, the special combination of elements may bring about the specificity of alloy properties.

The high entropy effect and slow diffusion effect keep the catalyst thermodynamically and kinetically stable, respectively, while the lattice distortion effect optimizes the electronic structure of the active site, and the cocktail effect produces a synergistic effect on metals.

3. Synthetic method

According to the process approach, the synthesis methods of HEAs can be divided into the 'bottom-up' preparation strategy by direct reaction of the solid phase, liquid phase and gas phase, and the 'top-down' preparation strategy through chemical or mechanical processes to dealloy or strip bulk materials to form nanostructures. The 'bottom-up' preparation method includes the carbon thermal shock method, moving bed pyrolysis method, magnetron sputtering method, electrodeposition method and wet chemical method, while the 'top-down' preparation method includes mechanical methods and the dealloying method.

3.1. Carbon thermal shock method

The carbon thermal shock method is an ultra-fast synthesis method for preparing mono-metal and multi-metal nanoparticles. Hu *et al.* first proposed a method to quickly heat the conductive carbon carrier loaded with a metal salt mixture to 2000–3000 K at a heating rate of 10^5 K s^{-1} under the protection of inert gas, forming uniform nanoparticles.[41] This method can effectively realize the high entropy of 15 elements and the controllable synthesis of single-phase alloy nanoparticles.[32] Xie *et al.* prepared CoMnFeNiCu HEA nanoparticles on oxygen-containing carriers by rapid heating and cooling.[49] The instantaneous high temperature can rapidly pyrolyze metal precursors and convert them into high-entropy metal droplets. Heat preservation in the millisecond range enables the metal droplets to maintain a dynamic balance of splitting and coalescence. Rapid cooling can reduce the diffusion behaviour between different elements. Carbon thermal shock technology can be used to quickly, efficiently and massively prepare HEA nanoparticles with uniform composition and uniform size, but it has certain requirements for the conductivity of the carrier.

3.2. Moving bed pyrolysis method

To overcome the dependence on the conductivity of the carrier, Lu *et al.* proposed a method for preparing HEAs by fast moving bed pyrolysis (FMBP).[22] They quickly put the metal precursor into a high-temperature tube furnace at 923 K within 5 s, and the mixed metal precursor was pyrolyzed at the same time to form HEA-NPs without phase separation (Fig. 2a). Compared with the sequential reduction of metal precursors in fixed bed pyrolysis (FBP), the mixed metal precursors in FMBP are instantaneously pyrolyzed, which ensures the high saturation of the monomer and the formation of smaller nuclear clusters (Fig. 2b). At present, FMBP has been used to synthesize ultra-small and highly dispersed HEAs composed of up to 10 immiscible elements. The low free energy of the nucleus and the rapid nucleation rate during the FMBP process ensure the formation of highly dispersed and uniform HEAs.[50]

3.3. Electrodeposition method

The electrodeposition method is a high-entropy material preparation technology by which metals or alloys from the compound solution deposit onto the conductive carrier. In 2018, Glasscott *et al.* proved that nanodroplet-mediated electrodeposition can effectively control the porosity of single Pt nanoparticles by introducing glycerol into water droplets.[51] In 2019, Glasscott *et al.* used this method to prepare high-entropy

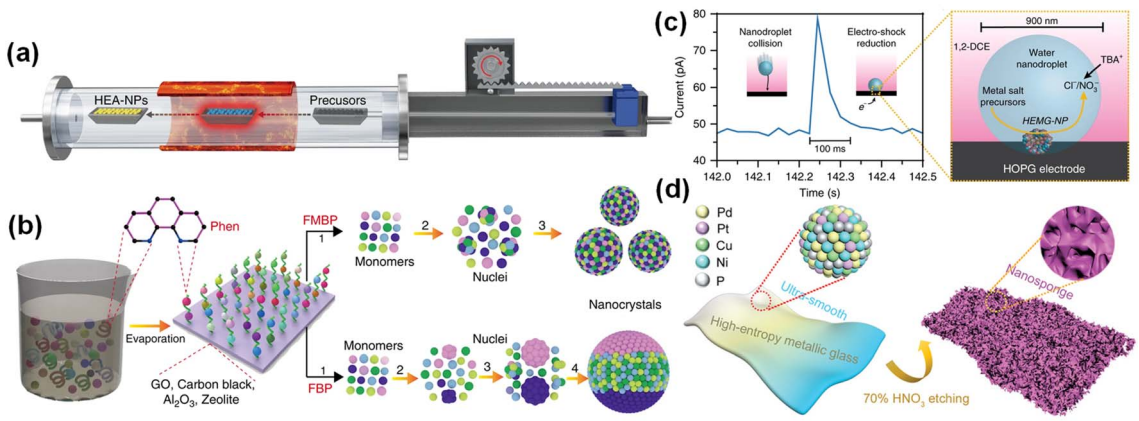

Fig. 2 (a) Schematic diagram of moving bed pyrolysis. (b) Synthesis of HEA-NPs by FMBP and FBP strategies. Reproduced with permission.[22] Copyright 2020, Springer Nature. (c) Nanodroplet-mediated electrodeposition method. Reproduced with permission.[20] Copyright 2019, Springer Nature. (d) The preparation process of nano-sponge HEMG. Reproduced with permission.[52] Copyright 2021, Wiley-VCH.

Open Access Article. Published on 19 ottobre 2023. Downloaded on 01/06/2026 19:16:00.
This article is licensed under a Creative Commons Attribution-NonCommercial 3.0 Unported Licence.

metallic glass (HEMG) with up to eight equimolar components, namely CoFeLaNiPtHEMG-NPs.[20] Specifically, mixing the aqueous solution of eight metal salt precursors in dichloroethane will form 'microreactors' in the microemulsion. At a cathodic potential of −1.5 V (*vs.* Ag/AgCl) and a pulse of about 100 ms (Fig. 2c), the metal ions were simultaneously reduced and deposited on a highly oriented pyrolytic graphite cathode electrode. This method is similar to the carbon thermal shock, but it is simpler than the carbon thermal shock method and can be carried out at room temperature.

3.4. Dealloying method

The dealloying method is based on the principle that non-active elements such as Al and Cu with lower electrode potentials are selectively removed, and the dissolved active metals are then formed by surface diffusion and self-assembly. Jia *et al.* used the dealloying method to effectively construct nanopores with high active surface sites and embedded crystal nano-sponge porous structures on NiCuPdPtP alloys, thereby providing more abundant active sites (Fig. 2d).[52] The lattice distortion and chemical complexity in high-entropy materials induce the transformation of electronic structure to reduce the energy barrier. Since the etching reaction usually occurs on the material surface, HEAs prepared by the dealloying method easily form metal/oxide or metal/hydroxide composite structures. Ding *et al.* prepared amorphous high-entropy oxide ultrathin core–shell nanostructures by the dealloying method.[53]

4. Characterization methods

Physical characterization is the key to exploring the physical and chemical properties of HEAs in electrocatalysis.[29] Zhang *et al.* summarized several characterization methods for HEAs to characterize their morphology, structure, surface state changes, and strain characteristics as shown in Fig. 3a.[54] This chapter mainly introduces advanced characterization methods for revealing the synergistic effect of HEAs in different reactions, such as *in situ* Raman and X-ray absorption fine structure (XAFS).

4.1. *In situ* Raman

Unlike traditional Raman, which can only detect the final product, *in situ* Raman can detect the intermediate product and the reaction process. Electrochemical *in situ* Raman can conveniently provide the microstructure information of the molecules on the electrode surface (interface). Wang *et al.* used *in situ* Raman to elucidate the surface structure transformation of CoNiCuMnAl@C in the overpotential range of 1.2–1.5 V (Fig. 3b and c).[55] Hao *et al.* revealed the adsorption of the reaction intermediates on the surface of FeCoNiMoRu HEA in

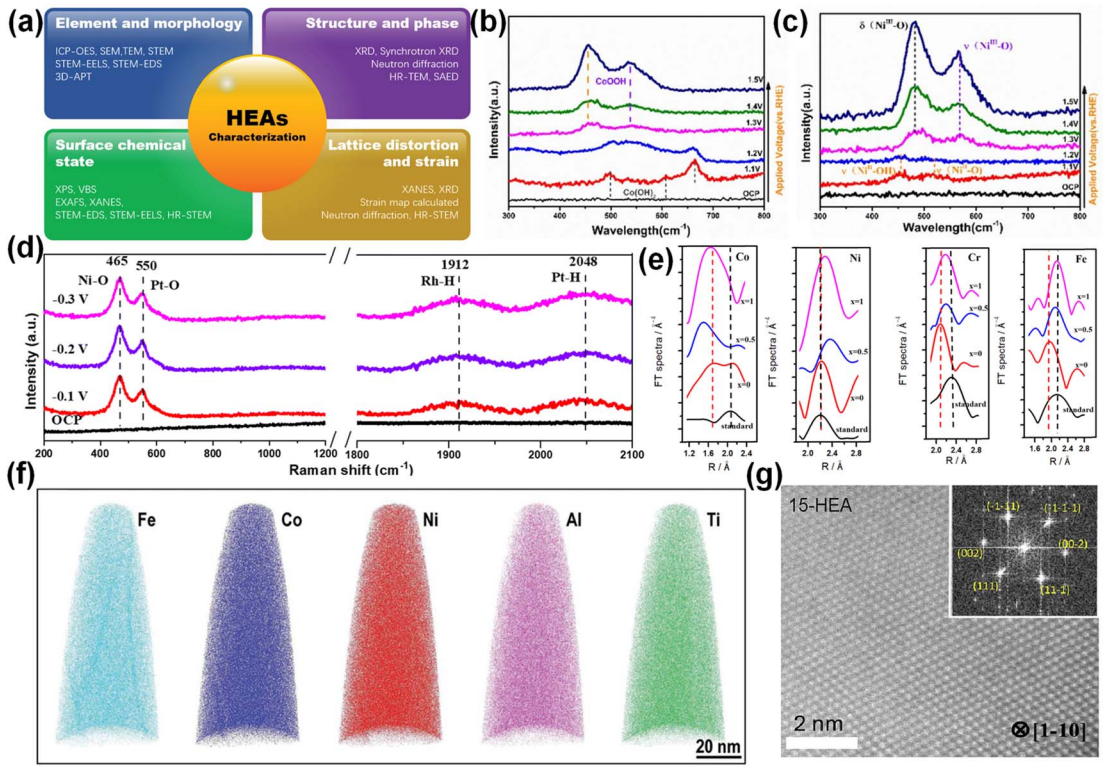

Fig. 3 (a) Various characterization techniques are summarized. Reproduced with permission.[54] Copyright 2022, Wiley-VCH. *In situ* Raman spectra of (b) CoCuMnAl@C and (c) CoNiCuMnAl@C. Reproduced with permission.[55] Copyright 2022, Elsevier Ltd. (d) *In situ* Raman of $Pt_{28}Mo_6Pd_{28}Rh_{27}Ni_{15}$ NCs. Reproduced with permission.[57] Copyright 2023, Royal Society of Chemistry. (e) Fourier transform spectra of XAFS K-edges in $AlCoCrFeNiW_x$. Reproduced with permission.[59] Copyright 2021, MDPI. (f) Element distribution shown by 3D-APT. Reproduced with permission.[60] Copyright 2020, Wiley-VCH. (g) Atomic-resolution HAADF image. Reproduced with permission.[32] Copyright 2021, Elsevier Ltd.

© 2023 The Author(s). Published by the Royal Society of Chemistry

Open Access Article. Published on 19 ottobre 2023. Downloaded on 01/06/2026 19:16:00.
This article is licensed under a Creative Commons Attribution-NonCommercial 3.0 Unported Licence.

the range of 0.1–1.5 V (*vs.* RHE) by *in situ* Raman.[56] When the applied potential increases from 0.2 V to 1.5 V, the peak intensities of N–H and C=O gradually increase, implying the continuous production of the HN–CO–NH intermediate. When the potential exceeds 1.2 V, the Ni site binds N element, Ru and Co stabilize C=O, and Fe–OH and Mo–OH are generated. After the C–N bond in the CON_2 intermediate is broken, two N atoms form N_2, and the remaining CO is attacked by OH– to form a CO_2 molecule. In FeCoNiMoRu HEA, the intermediates are stabilized by the integration effect between metals to improve the catalytic activity. Wei *et al.* determined that Pt and Ni are the direct active sites of hydrolysis dissociation in $Pt_{28}Mo_6Pd_{28}Rh_{27}Ni_{15}$ NCs by the *in situ* Raman technique, and Pt and Rh are the direct active sites of H* adsorption/desorption (Fig. 3d).[57]

4.2. XAFS

XAFS is mainly divided into XANES (X-ray absorption near edge structure) and EXAFS (extended X-ray absorption fine structure). When the spectral peak and shoulder of more than 20 to 30 eV are just passing through the starting point of the edge, the XANES region appears. The fine structure on the high-energy side of the edge where the energy decays to a few hundred electron volts is called EXAFS. Among them, XANES can be used to characterize the valence state of elements, d-band characteristics and atomic structure in catalysis. Tan *et al.* confirmed the severe oxidation of Mn in CrMnFeCoNi HEA by analyzing XANES spectra.[58] In addition, XANES also showed that Ni, Co and Fe atoms maintained similar crystal structures in the alloy, but the local short-range environment was slightly different. EXAFS can be used to study the coordination structure of atoms in HEAs and the chemical bond parameters between macromolecules. More importantly, it can be used to study the catalytic surface electronic structure changes. The difference of atomic radius and irregular atomic arrangement in HEAs will lead to lattice distortion. However, it is very difficult to characterize the lattice distortion in the experiment. Wu *et al.* verified the lattice distortion of AlCoCrFeNiW HEA by XAFS analysis.[59] As shown in Fig. 3e, the spectral positions of all elements in AlCoCrFeNiW HEA deviate from the standard sample, indicating that there is a huge lattice distortion. Among them, Co has a negative deviation and a large deviation, while Ni, Cr and Fe have similar positive deviations.

Other advanced characterization methods are also emerging. For example, 3D atomic probe tomography (3D-APT) is an element characterization technique that can visualize the distribution of elements and the formation of new phases at the atomic scale (Fig. 3f).[60] As early as 2015, Schuh *et al.* used 3D-APT to link the mechanical changes and microstructure of HEAs.[61] Zhao *et al.* studied the phase transformation, mechanical properties and phase transformation deformation behaviour of Ni–Co–Fe–Cr–Al–Nb HEA by combining 3D-APT and other characterization methods.[62] Atomic HR-STEM (high-resolution STEM) can be used to characterize the single-phase structure of HEAs (Fig. 3g).[32] High energy synchrotron X-ray and neutron diffraction can verify the existence of lattice distortion.[63] Aberration-corrected transmission electron microscopy (ACTEM) and high-angle annular dark field transmission electron microscopy (HAADF-STEM) can directly characterize the surface defects of HEAs. In addition, X-ray diffraction (XRD) can also detect defects through the original crystal structure and microcrystalline size.[64] With the continuous development of characterization technology, the reaction mechanism and structural changes of HEAs in electrocatalysis have been deeply understood, providing necessary conditions for their further design and applications.

5. The advantages of HEAs in electrocatalysis

HEAs have a highly disordered structure and a wide range of composition modulation, showing excellent performance in mechanical properties, magnetic properties and so on. In the future, HEAs are expected to become ideal catalytic materials in electrocatalytic reactions. Here, we systematically demonstrate why HEAs are considered as excellent electrocatalysts from the perspectives of abundant active sites, high selectivity, and high stability.

5.1. Abundant active sites

It is well known that ultradominant active sites determine the apparent activity of catalysts. Compared with single-atom catalysts and traditional alloys, the diversity of the number and types of metals in HEAs will produce a high degree of heterogeneity and different active sites, resulting in fast reaction kinetics. Jiang *et al.* prepared a nanoporous CuAlNiMoFe electrode, whose catalytic activity is about 46 and 14 times higher than that of CuNi and CuAlNi electrodes, respectively.[65] HEAs have higher catalytic activity perhaps due to their rich active sites and high configuration entropy. In addition, metal elements and their molar ratios also affect the number and local composition of active sites. Cui *et al.* proved that the overpotential of M_xS_y nanoparticles with one, two, three and four kinds of metal elements is inversely proportional to the number of metal elements (Fig. 4a).[66]

More importantly, the complex atomic mixing configuration makes HEAs possess multifunctional sites. In a monometallic catalyst, the single active site can only perform a specific reaction. In HEAs, multi-metal active sites can play a variety of roles, which can be used for various types of reactions. Huang *et al.* prepared PtRuNiCoFeMo HEA sub-nanowires (SNW) for alkaline hydrogen oxidation reaction (HOR).[67] The pin-on reaction at Fe and Mo sites, the highly stable valence state of Co and Ni sites, and the high activity of Pt and Ru sites contribute to the high performance of SNW, indicating that different metal sites have different effects (Fig. 4b). Kang *et al.* prepared $Pt_{34}Fe_5Ni_{20}Cu_{31}Mo_9Ru$ HEA with convex cubic nanocrystals (Fig. 4c).[68] In 1 M KOH, the overpotentials of $Pt_{34}Fe_5Ni_{20}Cu_{31}Mo_9Ru$ HEA for the HER and OER are 20 mV and 259 mV at 10 mA cm^{-2}, respectively. In 0.1 M $KClO_4$, the half-wave potential of $Pt_{34}Fe_5Ni_{20}Cu_{31}Mo_9Ru$ HEA for the ORR is 0.87 V *vs.* RHE. The excellent catalytic activity of the HEA in the HER, OER and ORR proves that multi-metal elements can be used for multiple types

Open Access Article. Published on 19 ottobre 2023. Downloaded on 01/06/2026 19:16:00.
This article is licensed under a Creative Commons Attribution-NonCommercial 3.0 Unported Licence.

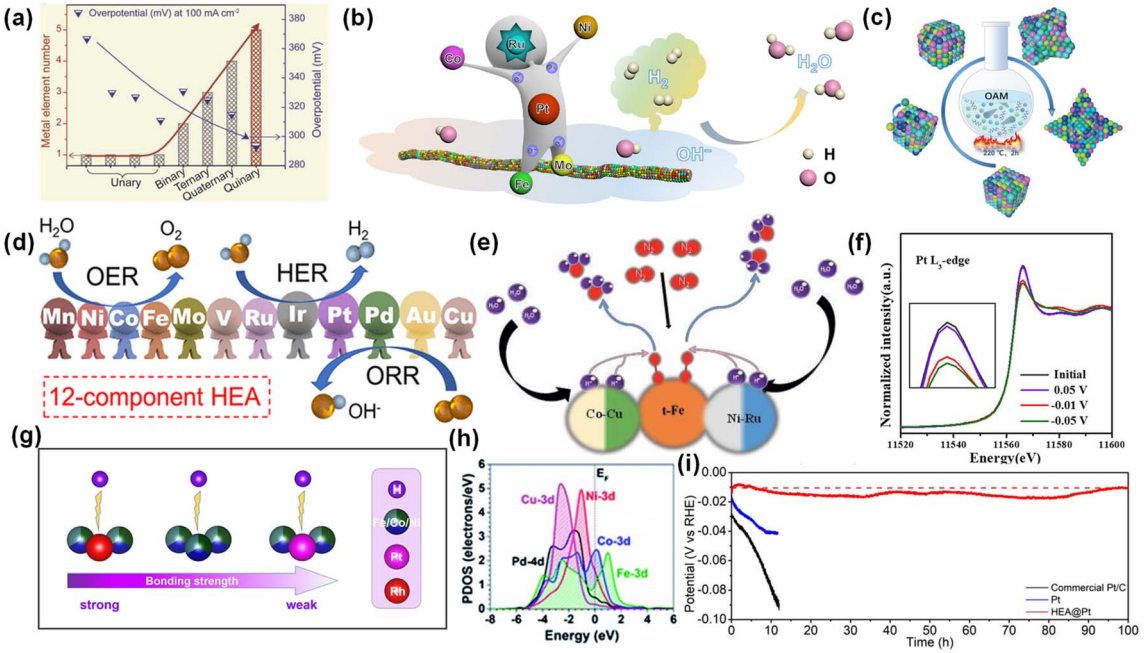

Fig. 4 (a) Comparison of overpotentials and metal element numbers. Reproduced with permission.[66] Copyright 2021, Wiley-VCH. (b) Schematic illustration of the HOR over HEA SNWs/C. Reproduced with permission.[67] Copyright 2021, Springer Nature. (c) Synthesis of $Pt_{34}Fe_5Ni_{20}Cu_{31}Mo_9Ru$ HEA. Reproduced with permission.[68] Copyright 2022, Wiley-VCH. (d) The application of np-12 in the HER, OER and ORR. Reproduced with permission.[69] Copyright 2022, American Chemical Society. (e) The mechanism diagram of RuFeCoNiCu NPs in the NRR. Reproduced with permission.[71] Copyright 2021, Wiley-VCH. (f) *In situ* normalized XANES spectra at the Pt L3-edge. (g) The binding strength of H to the Rh site, Fe–Co–Ni site and Pt site. Reproduced with permission.[18] Copyright 2021, American Chemical Society. (h) The projected density of states (PDOS) of the HEA surface. Reproduced with permission.[72] Copyright 2021, Royal Society of Chemistry. (i) The stability tests at 10 mA cm^{-2}. Reproduced with permission.[75] Copyright 2022, Wiley-VCH.

of reactions at the same time. Yu *et al.* used 12 metals, Mn, Ni, Co, Fe, Mo, V, Ru, Ir, Pt, Pd, Au and Cu, to form a multi-component nanoporous HEA (np-12).[69] np-12 exhibited high activity and durability for the HER, OER and ORR (Fig. 4d). The complex atomic configuration leads to the existence of multi-functional active sites in HEAs, which can be used for a variety of catalytic reactions.[70]

5.2. High selectivity

The synergistic effect between multiple metals not only regulates the electronic structure, but also provides various types of adsorption sites, which has strong application potential in multi-step tandem reactions (*e.g.* CO_2RR and NRR). Zhang *et al.* prepared RuFeCoNiCu HEA NPs for the NRR (Fig. 4e).[71] At a low overpotential of 0.05 V, the Faraday efficiency of the HEA NPs was 38.5%, and there was no significant attenuation after 100 h of continuous operation. DFT calculations showed that Fe in the HEA is the best site for N_2 adsorption and activation. Co–Cu and Ni–Ru couplings have excellent surface hydrogenation ability, making it easier for *H to activate N_2 to form NH_3. Biswas *et al.* prepared a CuPdAgPtAu HEA by low temperature ball milling for the CO_2RR.[19] The random distribution of elements in the HEA promoted the formation of active sites and optimized the adsorption energy of intermediate products, over which CO, CH_4 and C_2H_2 can be selectively produced. Therefore, the use of multi-metal component HEAs is an effective way to improve the CO_2RR kinetics and the selectivity of multi-carbon products.

5.3. Multi-site functionalization

The random distribution of various elements in a single phase will produce serious lattice distortion and inherent synergistic effects, which can regulate the electronic state and coordination environment.[70] Lei *et al.* prepared PdFeCoNiCu NPs for alkaline HER, which exhibited a low overpotential of 18 mV at 10 mA cm^{-2}.[72] DFT calculations showed that the synergistic effect between various metals in the HEA optimized the electronic structure. Specifically, HEA surface deformation led to surface electron modulation. Co and Ni sites showed high activity, which are the potential active sites in the initial water decomposition. Co helped to stabilize the adsorption of H_2O, while Ni contributed to the stability of *OH and the capture of protons at the Pd site. In addition, Pd and Cu have electron-rich properties. Among them, Pd enhanced the adsorption of free-moving protons, and Cu promoted electron transfer between metal sites. Fe enhanced the d–d electron coupling and compensated for the electrons at the Co position. The electronegativity difference between each metal causes the charge redistribution in HEAs, changes the d-band center position, and thus adjusts the adsorption energy of reactants and key intermediates.[73] The central position of the d band is crucial for the activity and selectivity of the catalyst. For example, for the HER, properly

© 2023 The Author(s). Published by the Royal Society of Chemistry

Open Access Article. Published on 19 ottobre 2023. Downloaded on 01/06/2026 19:16:00.
This article is licensed under a Creative Commons Attribution-NonCommercial 3.0 Unported Licence.

adjusting the d-band center of the H* binding site is beneficial to promote the dissociation of H, and the alloying between metals is beneficial to adjust the d-band center of the catalyst. Xia *et al.* prepared FeCoNiRhPt HEA nanoparticles (us-HEA) with a particle size of 2 nm for the HER.[18] In 0.5 M H_2SO_4, the η_{10} on us-HEA/C is only 27 mV. According to *in situ* XANES analysis, there was charge transfer between metal atoms in the HEA. The Pt site obtained electrons, and its Fermi level and d-band center were reduced, which optimized the hydrogen adsorption free energy (Fig. 4g and h).

5.4. Outstanding stability

The high mixing entropy makes HEAs tend to form a single solid solution phase, which makes it difficult to produce a potential difference between multiple phases and form a galvanic cell, thus improving the corrosion resistance of HEAs. At the same time, the transition elements (Al, Cr and Mo) make the alloy easy to passivate and form a passivation film, similar to the case of stainless steel. Hence, HEAs have better corrosion resistance than traditional alloys. Gao *et al.* prepared hollow HEA nanoparticles as cathode catalysts for Li–O_2 batteries.[74] The stability results showed that the hollow HEA remained intact after 80 cycles and more than 300 h cycles. Yao *et al.* used non-noble metal FeCoNiCu HEA nanoparticles to stabilize noble metal Pt and load it on carbonized wood.[75] As shown in Fig. 4i, HEA@Pt exhibited better stability than commercial Pt/C and Pt, and maintained the performance and structural stability after 100 h of continuous testing.

6. Theoretical study

HEAs have the complexity of composition and surface. It is difficult to find HEAs with suitable composition and structure by traditional repeated trial and error experimental methods. Computational methods (such as DFT, Monte Carlo, molecular dynamics, and artificial neural networks) have been widely used in monoatomic alloys,[76–79] ordered intermetallic alloys,[80] and surface and subsurface alloys.[81] In the past decade, research on machine learning (ML) has exploded, mainly because it can describe complex patterns. This function is of great help to solve the challenges faced by theoretical modelling of HEAs. From the simulation point of view, the calculation speed of ML is much faster than DFT, and it is closer to the empirical potential. In addition, ML can be used to identify the nonlinear structure–attribute relationship, which is conducive to a deeper exploration of the design space of HEAs.[82,83] Liu *et al.* used the ML method to establish the intrinsic correlation between local stacking fault energy and local composition inhomogeneity in HEAs, providing important guidance for the composition optimization.[84] Hou *et al.* proposed a hybrid framework of HEA phase prediction combining ML and empirical knowledge, which has high accuracy.[85]

In addition to studying the framework and properties of HEAs by theoretical calculations, great progress has been made in studying the thermodynamic/kinetic stability and adsorption energy of HEAs for electrocatalysis. Thermodynamic stability mainly depends on the enthalpy and entropy changes caused by element mixing. It is generally believed that HEAs can be formed when the conditions of atomic radius difference (δ) $\leq$ 6.6% and ratio of mixing entropy (S_{mix}) to mixing enthalpy (H_{mix}) (Ω) $\geq$ 1.1 are simultaneously satisfied. Batchelor *et al.* calculated 500 face-centered cubics containing 8 atoms to confirm that each structure of IrPdPtRhRu HEA falls in the region of $\delta \leq 6.6\%$ and $\Omega \geq 1.1$, indicating that it can maintain a single-phase solid solution state (Fig. 5a).[86]

Kinetic stability is used to measure the possibility of element diffusion and segregation in the catalytic process. Yao *et al.* simulated the kinetic stability of Ru-based multi-element alloy nanoparticles (MEA-NPs) by the mixed Monte Carlo-molecular dynamics (MC-MD) method.[42] They used five-membered $Ru_{0.25}Rh_{0.25}Co_{0.2}Ni_{0.2}Ir_{0.1}$ (about 4033 atoms) HEA nanoparticles to undergo two million MC diffusion steps at 1500 K, followed by high-temperature quenching to 298 K. The results

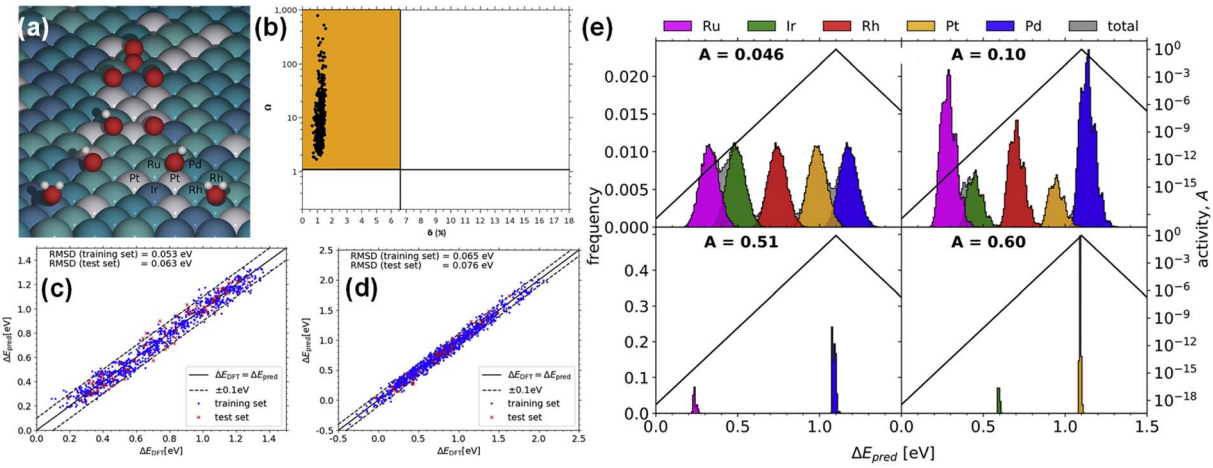

Fig. 5 (a) The chart of the Ω and δ of each 8-atom HEA unit cell. (b) A schematic diagram of *OH and *O adsorption on the IrPdPtRhRu surface. Predicted (c) *OH and (d) *O adsorption energies plotted against DFT-calculated energies. (e) Distribution of adsorption energies. Reproduced with permission.[86] Copyright 2019, Elsevier Ltd.

Open Access Article. Published on 19 ottobre 2023. Downloaded on 01/06/2026 19:16:00.
This article is licensed under a Creative Commons Attribution-NonCommercial 3.0 Unported Licence.

showed that the uniformly mixed alloy structure was not destroyed, indicating that it has dynamic stability. After that, they used the MD method to find that the self-diffusion coefficient is two orders of magnitude lower than that of $Ru_{0.25}Ni_{0.75}$, indicating that the lattice distortion caused by multi-element mixing has a hysteresis effect, thus maintaining its dynamic stability.

According to the Sabatier principle, the adsorption energy and catalytic activity of key intermediates often have a volcanic relationship.[87] When the adsorption energy reaches the optimum, the catalytic activity reaches the maximum. Batchelor *et al.* used a simple machine learning algorithm to predict the adsorption energy of the key intermediates (*OH and *O) of IrPdPtRhRu HEA in the ORR (Fig. 5b).[86] The predicted adsorption energies of *OH and *O are very close to the results of DFT calculations, with root mean square deviations of 0.063 and 0.076 eV (Fig. 5c and d), respectively. In addition, they found that the equimolar ratio of $Ir_{20}Pd_{20}Pt_{20}Rh_{20}Ru_{20}$ HEA has 2 times the activity of Pt (111), and the activity of $Ir_{10.2}Pd_{32.0}Pt_{9.30}Rh_{19.6}Ru_{28.9}$ is 5 times higher than that of Pt (111), on which the overpotential is 0.04 V (Fig. 5e). The adsorption energy of key intermediate products on the surface of high entropy alloys can be optimized by reasonable component design. Adsorption energy can also improve the selectivity of a specific product in some reactions. For example, in the CO_2RR, Cu has strong adsorption for CO and weak adsorption for H, and thereby Cu is the only metal that can form multi-carbon reduction products. Combining Cu with other metals to form HEAs can modulate the adsorption energy of different sites and improve the selectivity of multi-carbon reduction products.[88]

7. Applications of HEAs in electrocatalysis

The essence of a catalytic reaction is the process of adsorption and desorption of different intermediates. According to the volcano diagram, when the catalyst has a reasonable and moderate adsorption energy (corresponding to the vertex of the volcano diagram),[89] its catalytic activity is high. The widely adjustable adsorption energy range of HEAs formed by different elements can theoretically meet the essential requirements of electrocatalytic reactions, and the stability brought about by the accompanying high mixing entropy is favourable for the practical application. In this section, combined with the reports in recent years, we will analyze and summarize how to design HEAs according to the characteristics of different reactions.

7.1. Hydrogen evolution reaction

The HER mechanism is basically the same under acidic and alkaline conditions. The only difference is that the source of protons is different: under acidic conditions, protons are derived from H_3O^+, while under alkaline conditions, the proton comes from H_2O.[90] Taking alkaline conditions as an example, the process of HER mainly includes the adsorption and dissociation of water molecules, the generation and adsorption of H^+, and the generation and desorption of H_2. According to the Sabatier principle, the best catalytic activity can only be achieved when the intermediate adsorption reaches equilibrium.[87] The HER electrocatalytic volcano map was plotted by calculation as shown in Fig. 6a.[91] The noble metal Pt is the metal element closest to the vertex of the volcanic map, which is mainly due to its d_9 electronic structure with moderate intermediate adsorption energy. However, Pt is expensive and has low storage capacity, which is not conducive to industrial production.[92] In order to reduce the use of Pt metal, it is feasible to load Pt on high-entropy catalysts by electrodeposition to optimize the catalytic activity (Fig. 6b).[93] The synergistic effect between Pt and other metals optimizes the electron distribution of the catalyst and improves the utilization of the precious metal Pt. From Fig. 6a, for a single metal element, the positions of Pd and Pt on the volcano plot are close, indicating that the metal Pd also has high catalytic activity for the HER. Wang *et al.* prepared FeCoNiCuPd for the HER by magnetron sputtering and performed DFT calculations to explore the reaction mechanism.[15] According to the PDOS of each component in FeCoNiCuPd, Pd and Cu buried deep in E_f can be used as electronic memory (Fig. 6c). In addition, the Pd site is close to the E_f of the 4d orbital from the inside to the surface, which is beneficial to the adsorption of H* (Fig. 6d). Fig. 6e further confirms that Pd as an electronic memory can enhance the adsorption of H intermediates.

Defect engineering is often used to regulate the electronic structure of the catalyst, weaken the hydrogen binding energy, and improve the HER activity. Mao *et al.* prepared PdPtRhIrCu HEA with rich lattice distortion and defects by a simple hydrothermal synthesis method.[94] The overpotential of PdPtRhIrCu HEA at 10 mA cm^{-2} is only 15 mV, which is attributed to the ultra-thin high-entropy structure with lattice distortion and defects, which can provide ultra-high specific surface area, maximum atomic utilization and active surface metal atoms, thus promoting the adsorption and dissociation of reaction intermediates.

The alloying between non-precious metals can adjust the d-band center, thus affecting the intermediate adsorption capacity. The volcano plot of M–H bond energy based on Trasatti shows that Fe, Co and Ni on the left side and W on the right side have the best M–H bond energy.[95,96] Yao *et al.* confirmed that HEAs composed of Ni, Fe, Mo and Cu have the kinetics of enhancing hydrolysis and promoting the adsorption/desorption of active hydrogen intermediates (Fig. 6f and g). In addition, they introduced a Cu skeleton into HEAs, which not only promoted electron transfer, but also provided more channels to expose more active sites (Fig. 6h).[65] The phase structure of HEAs also affects their catalytic performance. Wang *et al.* enhanced the proportion of the BCC phase by increasing the proportion of Cr, which led to the relative downshift of the Fermi level of $Cr_{1.5}MnFeNi$ (Fig. 6i).[45] This will lead to the relative movement of the anti-bonding state and the weakening of the bonding, thereby fine-tuning the adsorption energy of HER intermediates. In addition to metal doping, the introduction of hetero-anions into HEAs can form corresponding compounds, such as oxides, nitrides, phosphide and sulfides, which is of great

© 2023 The Author(s). Published by the Royal Society of Chemistry

Open Access Article. Published on 19 ottobre 2023. Downloaded on 01/06/2026 19:16:00.
This article is licensed under a Creative Commons Attribution-NonCommercial 3.0 Unported Licence.

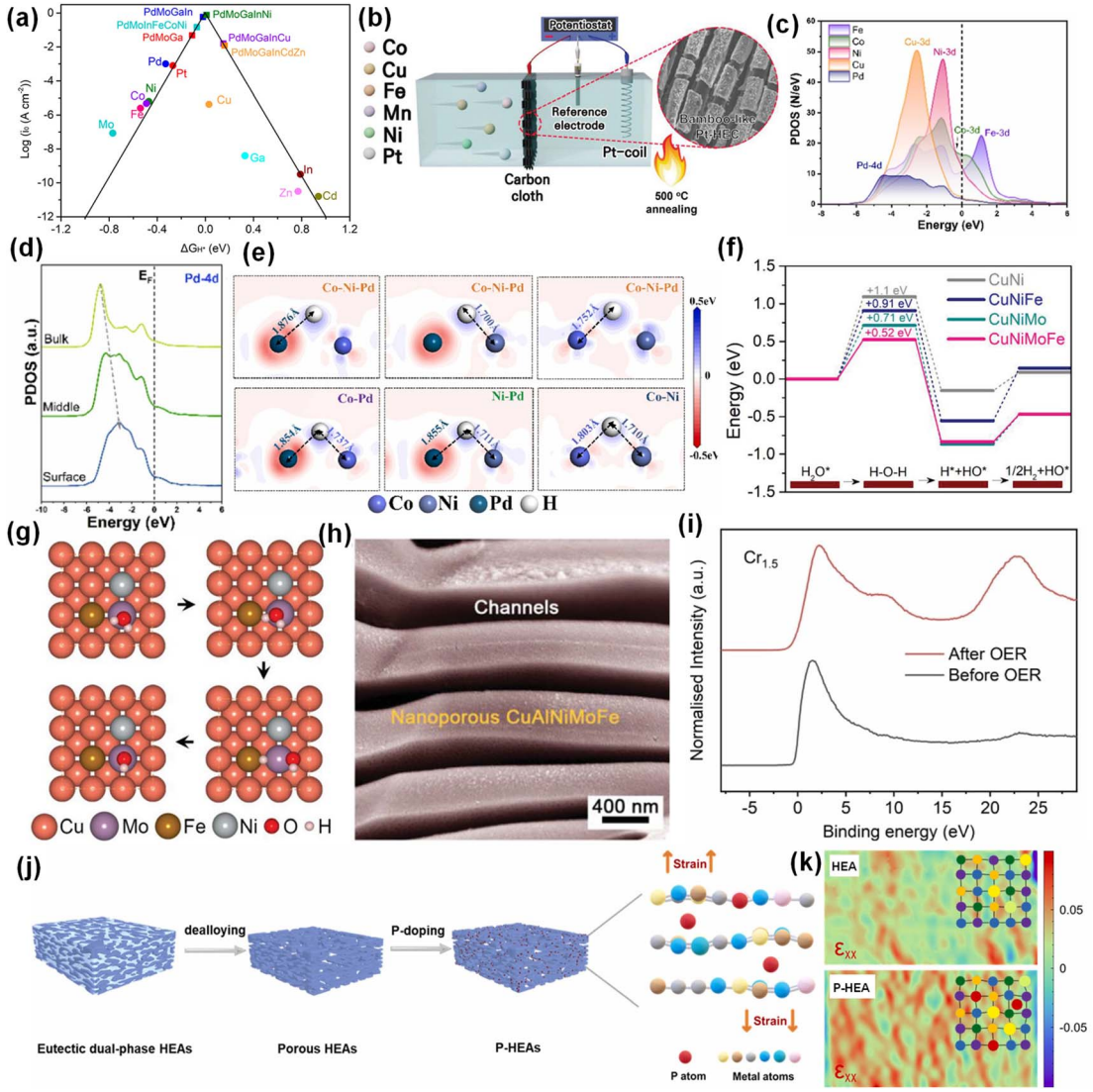

Fig. 6 (a) Volcano chart for the HER. Reproduced with permission.[91] Copyright 2022, American Chemical Society. (b) Loading Pt by electrodeposition. Reproduced with permission.[93] Copyright 2022, Wiley-VCH. (c) The PDOS. (d) The site-dependent PDOS of Pd. (e) DFT results of electron density difference between sites after H* adsorption. Reproduced with permission.[15] Copyright 2022, Elsevier Ltd. (f) Reaction energy diagram of water dissociation at different stages. (g) Surface configuration of the CuNiMoFe alloy. (h) SEM image of nanoporous CuAlNiMoFe. Reproduced with permission.[65] Copyright 2021, Wiley-VCH. (i) Normalized valence band spectra (VBS) of $Cr_{1.5}MnFeNi$. Reproduced with permission.[45] Copyright 2023, Elsevier Ltd. (j) Composite diagram of P-HEA. (k) Strain maps of HEA and P-HEA. Reproduced with permission.[97] Copyright 2023, Elsevier Ltd.

significance for adjusting the electronic structure and optimizing the adsorption energy of intermediates. Chen *et al.* doped atomic P into monolithic porous $Ni_{30}Co_{30}Fe_{10}Cr_{10}Al_{18}W_2$ HEA (Fig. 6j), which resulted in atomic lattice expansion and internal strain in the HEA.[97] In Fig. 6k, it is clearly observed that a P-doped HEA has wider lattice stretching strain distribution than the undoped HEA. DFT calculations showed that the electrons in P form a strong π-bond with the d orbital of the metal atom, which weakens the σ-bond between the H atom and metal atom. Different from common sense, in this experiment, the lattice expansion leads to the decrease of H adsorption energy and the easy desorption of H. The regulation of the internal lattice strain of HEAs by doping heteroatoms to optimize the electronic structure and intermediate adsorption energy provides feasibility for the preparation of high-efficiency HER catalysts. In conclusion, for the HER, the dissociation of water molecules and the adsorption of intermediate hydrogen are the key factors to be considered in the design of HEA catalysts.

7.2. Oxygen evolution reaction

The OER mainly involves the adsorption and desorption processes of HO*, O* and HOO* intermediates on the catalyst surface.[98] It is necessary to simultaneously improve the conductivity of the catalyst and increase the active adsorption sites to ensure that the electron and mass transport is not

Open Access Article. Published on 19 ottobre 2023. Downloaded on 01/06/2026 19:16:00.
This article is licensed under a Creative Commons Attribution-NonCommercial 3.0 Unported Licence.

limited. In acidic environments, Ir- and Ru-based materials are excellent electrocatalysts for anodic oxygen evolution,[99] while common low-cost non-precious metal catalysts are not applicable. Kwon *et al.* prepared ZnNiCoIrX (X = Fe or Mn) by using Ni and Co as effective alloying elements and Zn as a sacrificial element.[14] The combination of ZnNiCoMn adjusts the electronic structure of the Ir site and modifies the cohesive energy and adsorption energy. Due to the incorporation of Mn and the electronegativity difference between the elements, the total electron density increases. Fig. 7a and b show that the d-band electrons of Ir were rearranged with the incorporation of Mn, and the d-band structure of ZnNiCoIrMn became wider. The smaller $\Delta\varepsilon_d$ indicates that the more the anti-bonding state, the stronger the bonding force with the intermediate. ZnNiCoIrMn with a more negative d-band had a weaker hydrogen binding energy, which accelerated the desorption of H (Fig. 7c). Fig. 7d shows that the generation of HOO* was the rate-determining step of the OER, and the incorporation of Mn reduced the free energy of this step. The price of Ru is one-sixth that of Ir, and Ru has higher OER activity than Ir, but the stability of Ru-based catalysts under acidic conditions is a challenge. At present, the methods to improve the stability of Ru-based catalysts mainly include: (1) introducing interstitial carbon into Ru–O to extend the bond length,[100] (2) improving the formation energy of oxygen vacancies by heteroatom doping,[101] and (3) inhibiting lattice oxygen participation in the reaction.[102] The above methods are based on the adsorbent evolution mechanism (AEM). However, in recent years, the lattice oxygen oxidation mechanism (LOM) has received extensive attention. LOM involves the redox process of oxygen, directly generating the O–O chemical bond. Thereby, the LOM process can avoid the rate-determining step of O–O formation required for the AEM during the OER. Yu *et al.* selected transition metal elements (Ni^{2+}, Cr^{3+}, Fe^{3+}, Mo^{6+}) with similar atomic radii and different valence states to prepare $RuNiMoCrFeO_x$/CNT with oxygen vacancies by a solvent-free microwave method.[100] High entropy lattice oxygen participates in the reaction, and LOM dominates the OER process. $RuNiMoCrFeO_x$/CNT exhibited a low overpotential of 219 mV and 100 h stability in acidic electrolyte. The excellent performance comes from the high-entropy effect inhibiting element corrosion and excessive oxidation of lattice oxygen.

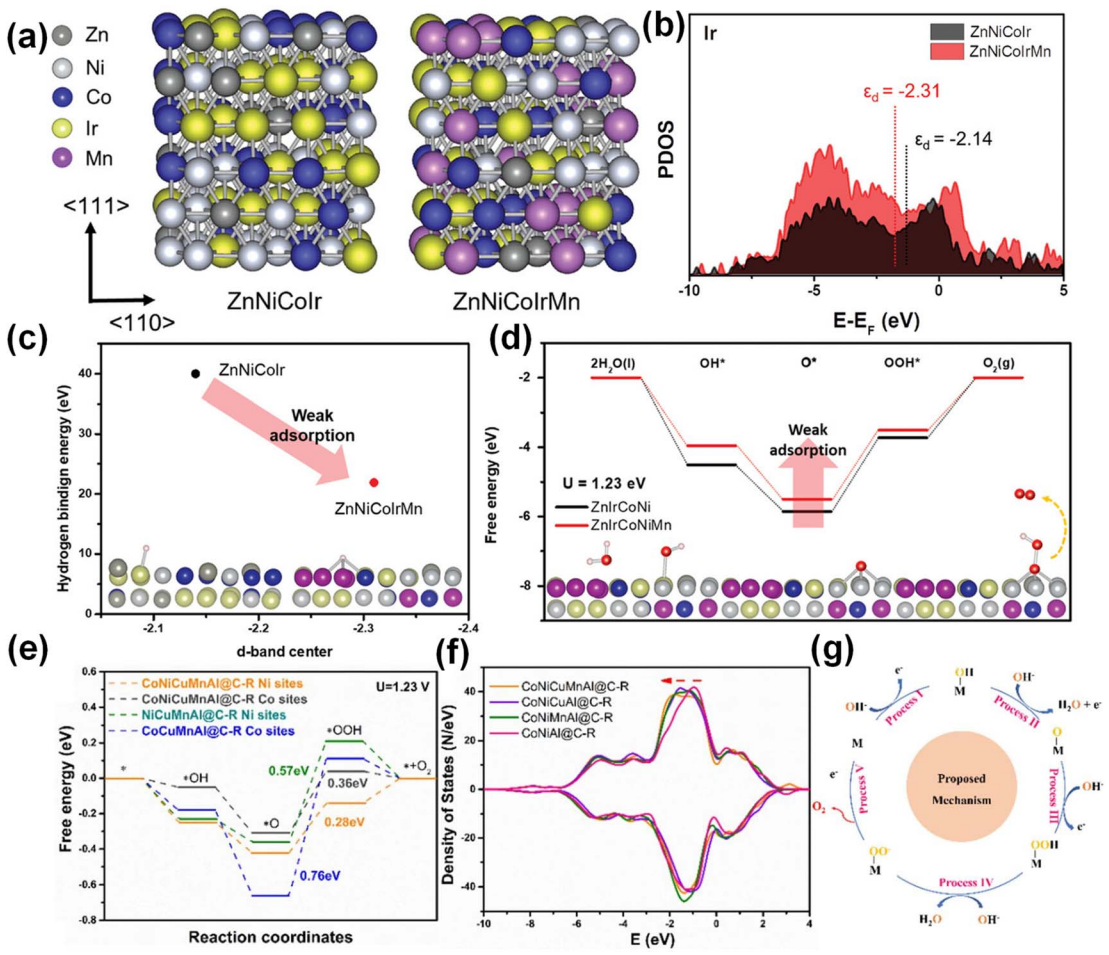

Fig. 7 (a) Computational modelling of ZnNiCoIr and ZnNiCoIrMn. (b) D-band projected DOS of Ir. (c) The linear relationship between the d-band center and hydrogen binding energy. (d) The energy diagram. Reproduced with permission.[14] Copyright 2023, Wiley-VCH. (e) Standard free energy diagram. (f) The d-orbital partial density of states. (g) The proposed OER mechanism. Reproduced with permission.[55] Copyright 2022, Elsevier Ltd.

© 2023 The Author(s). Published by the Royal Society of Chemistry

Open Access Article. Published on 19 ottobre 2023. Downloaded on 01/06/2026 19:16:00.
This article is licensed under a Creative Commons Attribution-NonCommercial 3.0 Unported Licence.

For non-precious metal catalysts, transition metals Ni, Fe and Co are electrocatalytically active substances, in which the activity of the metal center is highly correlated with the metal–oxygen bond. The increase of the metal oxidation state means that the electronegativity of the metal increases and the filling of the 3d orbital decreases, so that the 3d orbital overlaps with the 2p orbital of oxygen, the Fermi level decreases, and the OER overpotential reduces. Li *et al.* found that the addition of transition metals such as Cr, Mn, and V is beneficial to improve OER activity.[103] More importantly, the addition of Cr can promote higher oxidation state of active elements such as Co, Ni, and Fe, thereby reducing the OER overpotential. Wang *et al.* prepared nanoscale CoNiCuMnAl@C electrocatalysts by pyrolysis of CoNiCuMnAl-MOF precursors.[55] Studies have shown that the Ni/Co dual active sites synergistically accelerate the rate-determining step (O* → OOH*) (Fig. 7e), which helps to enhance the adsorption of key oxygen intermediates. The d-band center of Cu/Mn occupies the deeper position of the Fermi level and has the characteristic of being electron-rich, which helps to accelerate the electron transfer as electronic memory (Fig. 7f). The introduction of Al is beneficial to improve the conductivity of metal (oxygen) hydroxides and increase the active specific surface area. In addition, the thin carbon shell derived from the MOF template method is conducive to improving conductivity and promoting mass transfer. For the CoNiCuMnAl@C catalyst, the OER mechanism is shown in Fig. 7g.

Defects are of great help to optimize the adsorption and desorption of OER intermediates. Ren *et al.* prepared CrMnFeCoNi HEA with twin defects by means of a single metal doping quaternary system.[104] The introduction of metal elements distorts the lattice and produces dislocations, especially twins, leading to strong distortion and modulation of surface electronic states. DFT calculations showed that the presence of twin defects and lattice distortion reduces the energy barrier of the OER rate-determining step. The strain effect can induce lattice disorder, resulting in local reconstruction or mutation of atomic and electronic configurations on the catalyst surface, thus affecting the adsorption of oxygen intermediates.[105] The strain of the solid solution is mainly due to the uneven cooling rate during the preparation process. For example, the lattice will shrink during the low temperature process, and the atoms will deviate from the ideal position, which leads to the macroscopic and microscopic strain of the alloy. Zhang *et al.* prepared $Al_{0.6}CrFe_2Ni_2$ HEAs with strong lattice distortion.[106] The strain increases the charge transfer rate of OH adsorption in the OER. Based on the above research, non-precious metal elements such as Ni, Fe, Co, Cr, Mn, Cu, V and Al have OER catalytic activity, and the high entropy effect ensures that each metal exerts its own advantage to synergistically improve OER kinetics. In addition, strain engineering plays a key role in adjusting the electronic and geometric configurations of metal sites, thus promoting the OER.

7.3. Oxygen reduction reaction

The ORR process contains multiple steps and a variety of reaction intermediates, which is an important part of fuel cells and metal–air batteries.[107,108] The ORR involves a variety of intermediates, mainly including the initial reduction and decomposition of O_2^*, as well as the removal of adsorbed O*, HO* and H_2O* (Fig. 8a).[109] In the reaction process, the binding force between the catalyst and the reactant/intermediate is also the key to the catalytic activity. At present, the commercial catalyst is Pt/C, in which the content of platinum is usually 60–70%. Reducing the content of platinum will reduce the required electrocatalytic activity. Hence, researchers hope to improve the catalytic performance under the premise of reducing costs. Bimetallic PtM (PtCo, PtPd, PtNi, PtCu, *etc.*) composed of Pt alloy and transition metal can optimize the d-band center and adjust the electronic structure through the 'ligand effect' and 'strain effect'.[16] Unlike binary alloys, HEAs with complex composition due to the random distribution of atoms with different radii can regulate the electronic structure in a wider range, and can greatly reduce the use of precious metals and reduce costs. Chen *et al.* confirmed the synergistic effect and strain effect between Pt and other metals, and optimized the interaction between the catalyst and O*/OOH*.[68] For this reason, the half-wave potential of $Pt_{34}Fe_5Ni_{20}Cu_{32}Mo_9Ru$ under alkaline conditions was 0.86 V (Fig. 8b).

At present, the catalysts with Fe and Co as the active centers in non-noble metal ORR catalysts have the potential to replace noble metals. In addition, the inherent surface complexity of HEAs can provide nearly continuous adsorption energy and increase the proportion of active sites. Metal composition will affect the catalytic activity. He *et al.* prepared three high-entropy materials, CrMnFeCoNi, CuMnFeCoNi and MnFeCoNi, to verify the factors affecting the properties of HEAs.[104] The molecular configuration of the four basic steps of ORR on CrMnFeCoNi is shown in Fig. 8c. As shown in Fig. 8d, OH* to H_2O was the rate-determining step. Obviously, CrMnFeCoNi had the smallest rate-determining step energy barrier, while CuMnFeCoNi had the largest energy barrier. This means that the introduction of Cu causes the original ORR performance to deteriorate, while the introduction of Cr improves the original catalytic performance. In addition, lattice distortion affects the catalytic performance of HEAs. Fig. 8e shows that the d-band center of CrMnFeCoNi and CuMnFeCoNi with distortion moved down, and the binding energy with O_2 was reduced to promote the release of O_2. In order to improve the thermal stability, single-phase high-entropy oxides can be prepared by using similar ionic radii and electronic structure of transition metal elements.[110]

7.4. CO_2 reduction reaction

The electrocatalytic reduction of carbon dioxide to carbon-based fuels and chemicals can obtain a nearly closed-loop carbon cycle, which is necessary for mitigating climate change.[112] As shown in Fig. 8f and g, a variety of products can be produced during the CO_2RR, such as C_1 products (CO, CH_4, CH_3OH, and HCOOH), C_2 products (C_2H_4, C_2H_5OH, and CH_3COOH) and C_{2+} products (C_3H_7OH).[113] The reaction path involves more proton and electron coupling processes, and the selectivity of the product is difficult to adjust. Hence, the

Open Access Article. Published on 19 ottobre 2023. Downloaded on 01/06/2026 19:16:00.
This article is licensed under a Creative Commons Attribution-NonCommercial 3.0 Unported Licence.

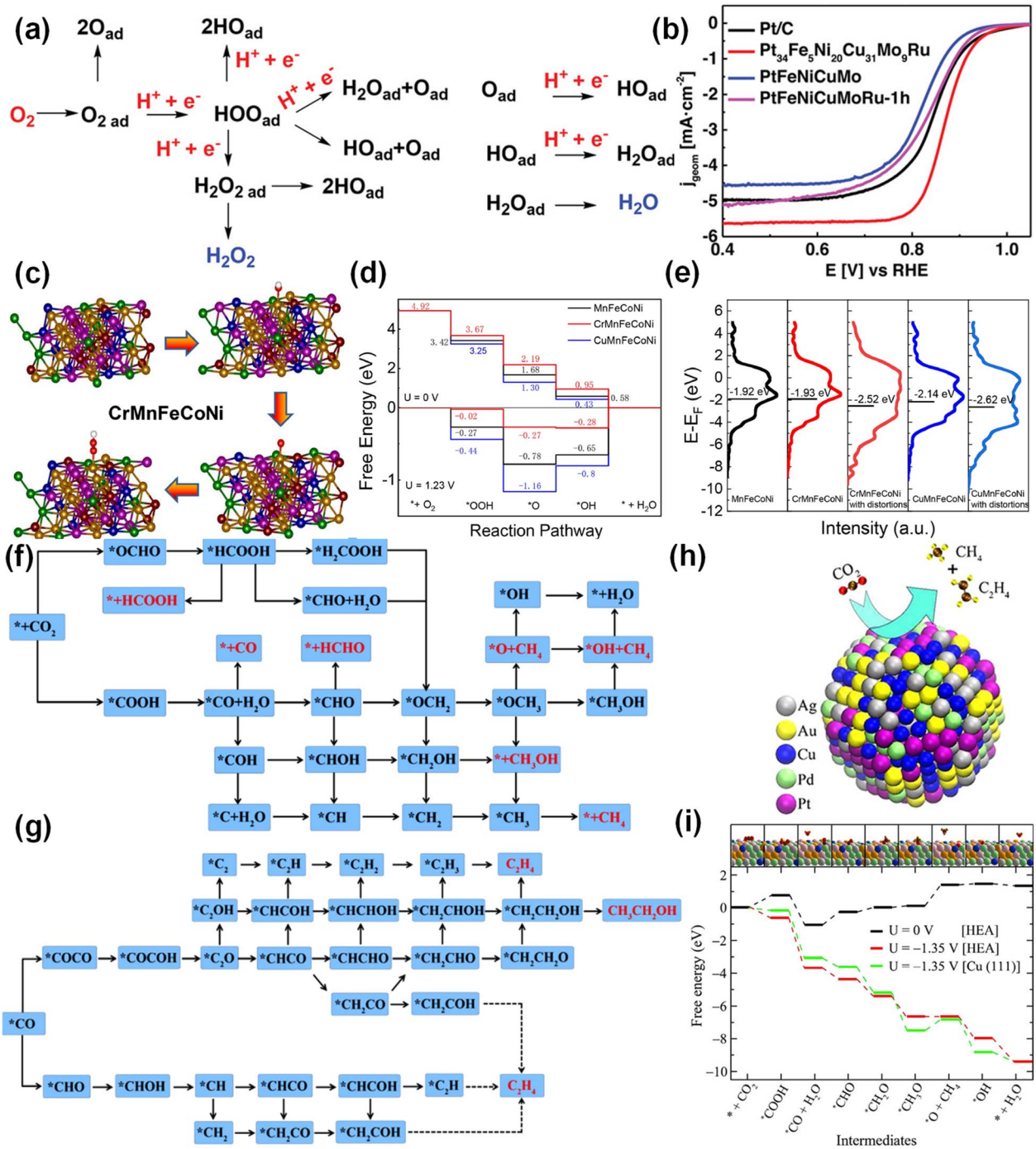

Fig. 8 (a) Schematic illustration of the possible ORR pathways. Reproduced with permission.[109] Copyright 2019, Wiley-VCH. (b) The polarization curve of $Pt_{34}Fe_5Ni_{20}Cu_{32}Mo_9Ru$. Reproduced with permission.[68] Copyright 2022, Wiley-VCH. (c) Atomic configuration of the four fundamental steps of the ORR. (d) Gibbs free energy change diagrams at 0 V and 1.23 V. (e) D-band spectra. Reproduced with permission.[104] Copyright 2023, Elsevier Ltd. (f and g) The possible reaction roadmap of CO_2. Reproduced with permission.[111] Copyright 2023, Royal Society of Chemistry. (g) The catalytic reaction diagram of AuAgPtPdCu. (h) Structure diagram of AuAgPtPdCu. (i) Free-energy diagram of the CO_2RR on the AuAgPtPdCu surface. Reproduced with permission.[19] Copyright 2020, American Chemical Society.

development of efficient electrocatalysts, optimization of the reaction kinetics of the rate-determining step, and improvement of the selectivity of multi-carbon products are the focus and difficulty of CO_2RR research. Cu is the only metal that can catalyze the selective reduction of CO_2 to high value-added multi-carbon products.[50] Biswas *et al.* prepared AuAgPtPdCu HEA nanoparticles for the CO_2RR (Fig. 8h).[19] The Faraday efficiency of gas products (CO, CH_4, C_2H_4 and H_2) is close to 100% at −0.3 V (*vs.* RHE). The randomly distributed metal elements promote the formation of a large number of active centers on

© 2023 The Author(s). Published by the Royal Society of Chemistry

Open Access Article. Published on 19 ottobre 2023. Downloaded on 01/06/2026 19:16:00.
This article is licensed under a Creative Commons Attribution-NonCommercial 3.0 Unported Licence.

the surface of HEAs, which is conducive to optimizing the adsorption and desorption of intermediates. Compared with the original Cu (111), AuAgPtPdCu HEAs optimize the binding energy of $*OCH_3$ and *O (Fig. 8i). The weaker $*OCH_3$ binding and the stronger *O binding promote the conversion of $*OCH_3$ to *O and stabilize the *O intermediate, thus showing better performance. The possibility of two-dimensional (2D) high-entropy materials exposing more active sites has great potential in catalytic applications. Cavin *et al.* prepared layered high-entropy transition metal disulfides using Mo, W, V, Nb and Ta metals.[114] DFT calculations showed that the 2D high-entropy metal sulfide had a multi-site synergistic catalytic effect. In addition, the V at the edge of the nanosheets optimized the CO desorption process. At present, the metal elements commonly used in electrocatalytic CO_2 reduction mainly include: (1) Au, Ag (the product is generally CO); (2) Pb, Sn, In and Bi (the products are generally formate); (3) Cu (the products are usually hydrocarbons); and (4) Pt, Ni (the products are usually hydrogen).[115,116] Polymetallic HEAs can provide multiple active sites, thereby enhancing electrocatalytic activity. In general, Cu is selected to form a multi-component alloy system with other metals, because Cu has a strong binding ability with CO. When CO is desorbed from other metal sites, it will bind to Cu sites, resulting in multi-carbon reduction products.[117]

7.5. Other reactions

The alcohol oxidation reaction (AOR) mainly includes the methanol oxidation reaction (MOR), ethanol oxidation reaction (EOR) and glycerol oxidation reaction (GOR).[118] The various reaction intermediates involved in the AOR require a multifunctional set of active sites. The interface of HEAs provides complex atomic configurations and different adsorption sites, which are conducive to the AOR. Chen *et al.* prepared PtRhBiSnSb nanosheets with hexagonal close-packed (hcp) crystal structure for the AOR by the wet chemical method.[119] The PtRhBiSnSb nanosheets have ultra-high mass activity of 19.529, 15.558 and 7.535 A mg_{Pt+Rh}^{-1} at the peak potentials of the MOR, EOR and GOR, respectively, mainly due to the synergistic effect between the five metals and the unique structural advantage of hcp. DFT calculations showed that the introduction of Rh optimizes the electronic structure, improves the electron transfer and increases the electroactivity of the optimal d-band center. The synergistic contribution of Bi, Sn and Sb makes Pt and Rh reach a robust valence state.

A direct formic acid fuel cell (DFAFC) is an efficient and environmentally friendly energy device. The reaction of anodic formic acid oxidation (FAO) is mainly divided into a direct pathway of direct oxidation of HCOOH to CO_2 and an indirect pathway of further oxidation of the CO intermediate state to CO_2 at high overpotential. Compared with Pt-based catalysts that are susceptible to CO poisoning, Pd-based catalysts generally do not involve a CO intermediate and are more abundant in reserves. Pd-based high-entropy alloying can not only enhance the utilization of Pd atoms, but also improve the stability and corrosion resistance by a high entropy and slow diffusion effect. Zuo *et al.* prepared a PdCuMoNiCo nano-hollow spherical HEA on carbon hybrids as a bifunctional catalyst for FAO and the ORR.[120] In it, Pd is the catalytic active center, and other elements act as cocatalysts to optimize the lattice parameters of Pd and regulate the adsorption energy of intermediates. The hydrogen fuel cell has the characteristics of high energy efficiency and no pollution, and is potential hydrogen power generation equipment. In this system, the H_2 oxidation reaction (HOR) occurs at the anode. Pt is currently the best catalyst for the HOR, but it is easily poisoned by CO. Pt-based HEAs have tunable electronic structure and entropy-stable properties. The mass activity of PtRuNiCoFeMo HEA subnanowires (SNW) can reach 6.75 A mg_{Pt+Rh}^{-1}, which is 4.1 times and 19.8 times that of commercial PtRu/C and Pt/C, respectively.[67] In addition, the resistance of PtRuNiCoFeMo HEA to CO poisoning was significantly enhanced. DFT calculations showed that the strong interaction between the metals in the HEA is beneficial to enhance HOR, where Pt and Ru are the real active centers. Fe and Mo sites can produce a pin-on effect, while Co and Ni maintain a highly stable valence.

The electrocatalytic nitrogen reduction reaction (NRR) is a new process to realize the green synthesis of ammonia. To date, the electrocatalytic NRR faces enormous challenges in both thermodynamics and kinetics. In addition, the HER as a competitive reaction reduces the selectivity of the NRR and the rate of ammonia production. N_2 has good bonding strength on metals such as Fe, Mo and Ru.[121] RuFeCoNiCu HEA NPs exhibited an NH_3 yield of 11.4 $\mu g\ h^{-1}\ cm^{-2}$ and Faraday efficiency of 38.5% at an overpotential of 0.05 V.[71] Theoretical calculations showed that Fe is the best site for N_2 adsorption and activation, and Co–Cu and Ni–Ru are coupled to exhibit excellent surface hydrogenation ability. Although there are few studies on HEAs for the above reactions currently, the high entropy of HEAs can not only regulate the electronic structure and optimize the d-band center, but also enhance the structural stability, thus exhibiting broad prospects.

8. Regulation strategies for HEAs

8.1. Element regulation

According to the reaction system, metal elements with unique properties are selected to optimize the selectivity and activity of the catalyst. Miracle *et al.* summarized the frequency of use of individual metals in HEAs as shown in Fig. 9a, where the vertical line is proportional to the number of uses.[48] Fe, Co, Ni, Mn, Cr, Cu, Al and Ti are the most commonly used elements. As mentioned above, Pt and Pd are the best HER elements;[1,12] Ir and Ru are the best OER elements;[122,123] and Cu is the only metal that can catalyze the selective reduction of CO_2 to high value-added multi-carbon products.[124] More importantly, HEAs are a good choice for bifunctional and multifunctional catalysis. For example, Ni, Co, Fe and Pt are often used to prepare highly active bifunctional HEAs for the HER and OER.[15,125,126] The coordination between multiple metals is beneficial to optimize the electron density and adjust the adsorption strength, usually exhibiting higher performance than single-component metals.

Open Access Article. Published on 19 ottobre 2023. Downloaded on 01/06/2026 19:16:00.
This article is licensed under a Creative Commons Attribution-NonCommercial 3.0 Unported Licence.

8.2. Defect regulation

When multiple structural units (including atoms and molecules) are incorrectly arranged, defects will be generated, which can regulate the adsorption and electronic structure of the catalyst (Fig. 9b).[127] Defects are thermodynamically unstable due to high free energy, and are more likely to adsorb reactants, thus becoming catalytic active sites.[64] There are many kinds of surface defects such as vacancies, dislocations and grain boundaries in HEAs, which is mainly due to the complexity of the structure and composition elements.[128] Defect engineering is an important and effective strategy to improve catalytic activity. Yang *et al.* used magnetron sputtering technology to create defects in HEA films, which was conducive to the formation of more active sites.[24,129] In addition, high-energy particles in plasma technology (plasma etching, doping and vacancy) attack the HEA surface (Fig. 9c), which not only destroys chemical bonds, but also produces new chemical bonds, thereby etching and modifying the HEA surface.[130,131] The dealloying technology can realize reasonable control of the surface nanostructure. Kruzic *et al.* used this method to obtain a high-entropy metallic glass (HEMG) with a nano-sponge structure.[52] DFT calculations showed that the lattice distortion and chemical complexity of nanocrystals stabilized the adsorption and desorption of H*, which was beneficial to improve HER activity (Fig. 9d).

8.3. Strain engineering

Strain changes the original state of the atomic bond by stretching or compressing the distance of the chemical bond and changing the lattice symmetry.[132] Multi-component HEAs are more likely to produce lattice strain due to different lattice parameters. Wu *et al.* studied the strain effect of Fe, Co, Ni, Pd and Pt by DFT simulations.[133] Under low refractive index (110) and (100) surfaces (Fig. 9e), Ni and Co follow the conventional prediction of strain effect, while Fe, Pd and Pt do not. This indicates that phase transition may be achieved by precise strain modulation, which is an important reference for the study of electrocatalytic fine modulation of HEAs in the future. The tensile strain will make the d-band center move up, while the compressive strain makes the d-band center move down.[134] The upward shift of the center of the d band will enhance the adsorption energy of the intermediate.[54] Wang *et al.* heated PtFeCoNiCu HEAs at 400 °C and 700 °C to produce different degrees of strain.[135] The HEA heated at 400 °C showed stronger compressive strain, which made the d-band center move down.

9. Summary and prospects

HEAs have shown more and more obvious potential in electrocatalytic research due to their excellent combined properties. In the future, HEAs may become the center of the field of structural and functional materials. This review introduces the concept of HEAs and summarizes the main synthesis methods and how to design and prepare HEA catalysts for electrochemical reactions such as the HER, HOR, OER, ORR, CO_2RR, NRR and AOR. The multi-element alloy combining the characteristics of site-occupancy disorder and lattice order can optimize the surface electronic structures of HEAs, thus exhibiting better catalytic performance than the corresponding low-element system.[86] In addition, the strength of adsorption energy can be affected by adjusting the kind and the proportion of metal elements.[136] Electrocatalytic HER, HOR, OER, ORR, CO_2RR, NRR and AOR involve multi-step reactions, and the uniform distribution of multiple active sites on the surface of the catalyst can break the limitation of interdependence, which is beneficial to adjust the binding energy and improve the catalytic activity.[137,138]

Although HEAs are considered to be promising electrocatalysts, studies are still limited to the exploration of synthetic methods and the screening of element combinations. There are still many challenges in the research of the catalytic mechanism and practical applications. For example, it is hard to achieve precise shape control of HEAs, and the precise occupancy

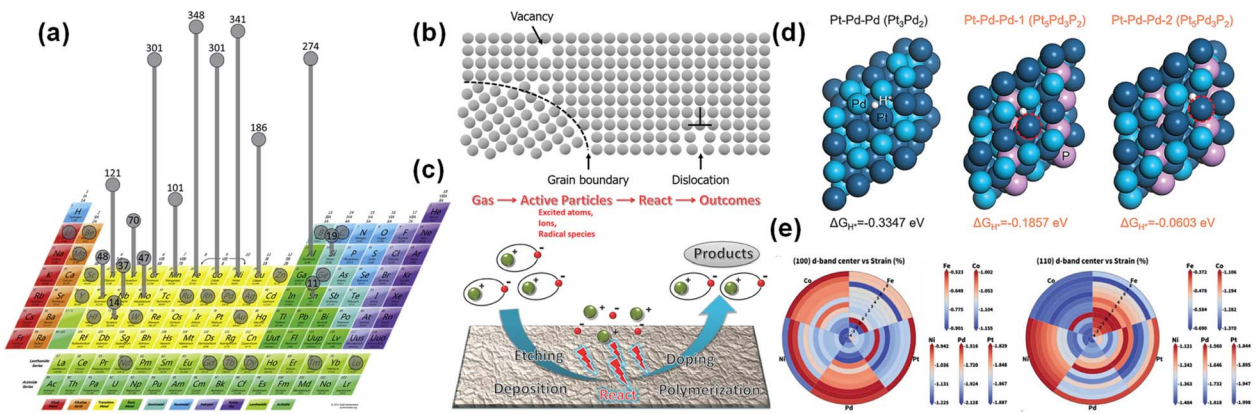

Fig. 9 (a) The frequency of elements used in the 408 multi-component alloys (MPEAs) evaluated. Reproduced with permission.[48] Copyright 2017, Elsevier Ltd. (b) Common defects in HEAs. Reproduced with permission.[127] Copyright 2019, Elsevier Ltd. (c) Plasma technology schematic diagram. Reproduced with permission.[130] Copyright 2018, Wiley-VCH. (d) Local chemical environment of H* adsorption. Reproduced with permission.[52] Copyright 2021, Wiley-VCH. (e) Comparing the heat map of the effect of (110) and (100) strains on the depth change of the d-band center. Reproduced with permission.[133] Copyright 2020, Wiley-VCH.

© 2023 The Author(s). Published by the Royal Society of Chemistry

Open Access Article. Published on 19 ottobre 2023. Downloaded on 01/06/2026 19:16:00.
This article is licensed under a Creative Commons Attribution-NonCommercial 3.0 Unported Licence.

control of local atoms in HEAs is not enough. In addition, although the morphology, crystal structure and element distribution in HEAs can be well characterized, there is still no definite evidence for the specific relationship between the structure and electrocatalytic performance. Finally, due to the complexity of the surface and internal structure of HEAs and multi-step reactions involved in electrocatalysis, the understanding of the catalytic structure–activity relationship of HEAs is still unclear.

To cope with the above difficulties and challenges and better understand the mechanisms of HEAs in electrocatalysis, the following research directions are proposed. First of all, the combination of theory and experiment is very important to understand the catalytic mechanisms of HEAs. It is the focus of future research to develop new calculation software or models and new calculation methods to determine the dynamic evolution process of active sites in HEAs and the influencing mechanism of other effects on performance. Secondly, precise control of the composition and size of HEAs can afford abundant active sites, favouring electrocatalytic reactions. The structural characterization of the microscopic inhomogeneity and surface atomic resolution of HEAs should be strengthened, including chemical valence and local stress distribution. Phase engineering may enable HEAs with the same composition to exhibit different crystal structures under different conditions. Finally, HEAs need further expansion, such as the design of composite materials with a core–shell structure or interface structure. These materials may have potential applications in catalysis or other fields.

Author contributions

All of the authors contributed to the literature search, writing and editing of this review.

Conflicts of interest

There are no conflicts to declare.

Acknowledgements

This work was supported by the National Natural Science Foundation of China (No. 22075099), the Natural Science Foundation of Jilin Province (No. 20220101051JC), and the Education Department of Jilin Province (No. JJKH20220968CY).

Notes and references

1 T. Tang, Z. Wang and J. Guan, *Coord. Chem. Rev.*, 2023, **492**, 215288.
2 X. Bai and J. Guan, *Small Struct.*, 2023, **4**, 2200354.
3 Y. Guo, B. Hou, X. Cui, X. Liu, X. Tong and N. Yang, *Adv. Energy Mater.*, 2022, **12**, 2201548.
4 P. Tang, P.-Y. Huang, J. E. N. Swallow, C. Wang, D. Gianolio, H. Guo, J. H. Warner, R. S. Weatherup and M. Pasta, *ACS Catal.*, 2023, **13**, 9558–9566.
5 X. Bai, J. Han, X. Niu and J. Guan, *Nano Res.*, 2023, **16**, 10796–10802.
6 J. Han and J. Guan, *Nano Res.*, 2023, **16**, 1913–1966.
7 Y. Wang, W. Nong, N. Gong, T. Salim, M. Luo, T. L. Tan, K. Hippalgaonkar, Z. Liu and Y. Huang, *Small*, 2022, **18**, 2203340.
8 X. Bai and J. Guan, *Chin. J. Catal.*, 2022, **43**, 2057–2090.
9 X. Bai, Y. Wang, J. Han, X. Niu and J. Guan, *Appl. Catal., B*, 2023, **337**, 122966.
10 T. Tang, Y. Wang, J. Han, Q. Zhang, X. Bai, X. Niu, Z. Wang and J. Guan, *Chin. J. Catal.*, 2023, **46**, 48–55.
11 L. Xiao, Z. Wang and J. Guan, *Coord. Chem. Rev.*, 2022, **472**, 214777.
12 D. Jin, F. Qiao, H. Chu and Y. Xie, *Nanoscale*, 2023, **15**, 7202–7226.
13 Y. Zhou, X. Shen, M. Wang, L. Zhang, T. Qian, C. Yan and J. Lu, *Sci. China Mater.*, 2023, **66**, 2527–2544.
14 J. Kwon, S. Sun, S. Choi, K. Lee, S. Jo, K. Park, Y. K. Kim, H. B. Park, H. Y. Park, J. H. Jang, H. Han, U. Paik and T. Song, *Adv. Mater.*, 2023, **35**, 2300091.
15 S. Wang, B. Xu, W. Huo, H. Feng, X. Zhou, F. Fang, Z. Xie, J. K. Shang and J. Jiang, *Appl. Catal., B*, 2022, **313**, 121472.
16 J. Shen, Z. Hu, K. Chen, C. Chen, Y. Zhu and C. Li, *Mater. Today Nano*, 2023, **21**, 100282.
17 L. Liu, H. Akhoundzadeh, M. Li and H. Huang, *Small Methods*, 2023, 2300482.
18 G. Feng, F. Ning, J. Song, H. Shang, K. Zhang, Z. Ding, P. Gao, W. Chu and D. Xia, *J. Am. Chem. Soc.*, 2021, **143**, 17117–17127.
19 S. Nellaiappan, N. K. Katiyar, R. Kumar, A. Parui, K. D. Malviya, K. G. Pradeep, A. K. Singh, S. Sharma, C. S. Tiwary and K. Biswas, *ACS Catal.*, 2020, **10**, 3658–3663.
20 M. W. Glasscott, A. D. Pendergast, S. Goines, A. R. Bishop, A. T. Hoang, C. Renault and J. E. Dick, *Nat. Commun.*, 2019, **10**, 2650.
21 H.-J. Qiu, G. Fang, J. Gao, Y. Wen, J. Lv, H. Li, G. Xie, X. Liu and S. Sun, *ACS Mater. Lett.*, 2019, **1**, 526–533.
22 S. Gao, S. Hao, Z. Huang, Y. Yuan, S. Han, L. Lei, X. Zhang, R. Shahbazian-Yassar and J. Lu, *Nat. Commun.*, 2020, **11**, 2016.
23 P. A. Sukkurji, Y. Cui, S. Lee, K. Wang, R. Azmi, A. Sarkar, S. Indris, S. S. Bhattacharya, R. Kruk, H. Hahn, Q. Wang, M. Botros and B. Breitung, *J. Mater. Chem. A*, 2021, **9**, 8998–9009.
24 P. Yang, Y. Shi, T. Xia, Z. Jiang, X. Ren, L. Liang, Q. Shao and K. Zhu, *J. Alloys Compd.*, 2023, **938**, 168582.
25 H. Wu, Q. Lu, Y. Li, J. Wang, Y. Li, R. Jiang, J. Zhang, X. Zheng, X. Han, N. Zhao, J. Li, Y. Deng and W. Hu, *Nano Lett.*, 2022, **22**, 6492–6500.
26 Y. Wang, H. Yang, Z. Zhang, X. Meng, T. Cheng, G. Qin and S. Li, *J. Mater. Sci. Technol.*, 2023, **166**, 234–240.
27 H. Pérez Blanes, P. Ghiasi, J. Sandkühler, Y. Yesilcicek, S. Pentzien, A. Conradi, C. Prinz, D. Al-Sabbagh, A. F. Thünemann, O. Ozcan and J. Witt, *J. Mater. Res. Technol.*, 2023, **24**, 9434–9440.
28 S. A. Lee, J. Bu, J. Lee and H. W. Jang, *Small Sci.*, 2023, **3**, 2200109.

Open Access Article. Published on 19 ottobre 2023. Downloaded on 01/06/2026 19:16:00.
This article is licensed under a Creative Commons Attribution-NonCommercial 3.0 Unported Licence.

29 X. Han, G. Wu, S. Zhao, J. Guo, M. Yan, X. Hong and D. Wang, *Matter*, 2023, **6**, 1717–1751.
30 J. W. Yeh, S. K. Chen, S. J. Lin, J. Y. Gan, T. S. Chin, T. T. Shun, C. H. Tsau and S. Y. Chang, *Adv. Eng. Mater.*, 2004, **6**, 299–303.
31 B. Cantor, I. T. H. Chang, P. Knight and A. J. B. Vincent, *Mater. Sci. Eng., A*, 2004, **375**, 213–218.
32 Y. Yao, Z. Huang, L. A. Hughes, J. Gao, T. Li, D. Morris, S. E. Zeltmann, B. H. Savitzky, C. Ophus, Y. Z. Finfrock, Q. Dong, M. Jiao, Y. Mao, M. Chi, P. Zhang, J. Li, A. M. Minor, R. Shahbazian-Yassar and L. Hu, *Matter*, 2021, **4**, 2340–2353.
33 Y. F. Ye, Q. Wang, J. Lu, C. T. Liu and Y. Yang, *Mater. Today*, 2016, **19**, 349–362.
34 Y.-G. Tong, N. Tian, H.-F. Huang, Z.-B. Zhang, X.-B. Liang, X.-X. Ji, J.-Z. Fang and Y.-L. Hu, *Rare Met.*, 2023, **42**, 2020–2027.
35 X. Wei, L. Zhang, C. Zhang and G. Li, *Mater. Lett.*, 2023, **339**, 134107.
36 B. Akhil, A. Bajpai and K. Biswas, *Philos. Mag. Lett.*, 2022, **102**, 287–298.
37 S. H. Hong, H. J. Park, G. C. Kang, Y. S. Kim, G. Song and K. B. Kim, *Scr. Mater.*, 2022, **209**, 114391.
38 J. Zhang, C. Zhao, Y. Wu, C. Chen, Z. Chen and B. Shen, *Acta Metall. Sin.*, 2022, **58**, 215–224.
39 J.-K. Xiao, H. Tan, Y.-Q. Wu, J. Chen and C. Zhang, *Surf. Coat. Technol.*, 2020, **385**, 125430.
40 Y. Lu, X. Zhang, H. Wang, C. Kan, F. Zhang, P. Dai and H. Wang, *Mater. Charact.*, 2022, **189**, 111959.
41 Y. Yao, Z. Huang, P. Xie, S. D. Lacey, R. J. Jacob, H. Xie, F. Chen, A. Nie, T. Pu, M. Rehwoldt, D. Yu, M. R. Zachariah, C. Wang, R. Shahbazian-Yassar, J. Li and L. Hu, *Science*, 2018, **359**, 1489–1494.
42 Y. Yao, Z. Liu, P. Xie, Z. Huang, T. Li, D. Morris, Z. Finfrock, J. Zhou, M. Jiao, J. Gao, Y. Mao, J. Miao, P. Zhang, R. Shahbazian-Yassar, C. Wang, G. Wang and L. Hu, *Sci. Adv.*, 2020, **6**, eaaz0510.
43 Y. Tian, W. Zhou, M. Wu, H. Luo, Q. Tan, G. Zhu, A. Dong, D. Shu and B. Sun, *J. Alloys Compd.*, 2022, **915**, 165324.
44 J. Huang, P. Wang, P. Li, H. Yin and D. Wang, *J. Mater. Sci. Technol.*, 2021, **93**, 110–118.
45 Y. Wang, N. Gong, G. Niu, J. Ge, X. Tan, M. Zhang, H. Liu, H. Wu, T. L. Meng, H. Xie, K. Hippalgaonkar, Z. Liu and Y. Huang, *J. Alloys Compd.*, 2023, **960**, 171039.
46 K. Zhao, X. Li and D. Su, *Acta Phys.-Chim. Sin.*, 2021, **37**, 2009077.
47 J.-W. Yeh, S.-Y. Chang, Y.-D. Hong, S.-K. Chen and S.-J. Lin, *Mater. Chem. Phys.*, 2007, **103**, 41–46.
48 D. B. Miracle and O. N. Senkov, *Acta Mater.*, 2017, **122**, 448–511.
49 P. Xie, Y. Yao, Z. Huang, Z. Liu, J. Zhang, T. Li, G. Wang, R. Shahbazian-Yassar, L. Hu and C. Wang, *Nat. Commun.*, 2019, **10**, 4011.
50 K. Li and W. Chen, *Mater. Today Energy*, 2021, **20**, 100638.
51 M. W. Glasscott and J. E. Dick, *ACS Nano*, 2019, **13**, 4572–4581.
52 Z. Jia, K. Nomoto, Q. Wang, C. Kong, L. Sun, L.-C. Zhang, S.-X. Liang, J. Lu and J. J. Kruzic, *Adv. Funct. Mater.*, 2021, **31**, 2101586.
53 Z. Ding, J. Bian, S. Shuang, X. Liu, Y. Hu, C. Sun and Y. Yang, *Adv. Sustainable Syst.*, 2020, **4**, 1900105.
54 Y. Zhang, D. Wang and S. Wang, *Small*, 2022, **18**, 2104339.
55 S. Wang, W. Huo, F. Fang, Z. Xie, J. K. Shang and J. Jiang, *Chem. Eng. J.*, 2022, **429**, 132410.
56 J. Hao, J. Li, Y. Zhu, S. Sun, S. Lu, M. Du and H. Zhu, *Chem. Commun.*, 2023, **59**, 772–775.
57 M. Wei, Y. Sun, J. Zhang, F. Ai, S. Xi and J. Wang, *Energy Environ. Sci.*, 2023, **16**, 4009–4019.
58 Y.-Y. Tan, M.-Y. Su, Z.-C. Xie, Z.-J. Chen, Y. Gong, L.-R. Zheng, Z. Shi, G. Mo, Y. Li, L.-W. Li, H.-Y. Wang and L.-H. Dai, *Intermetallics*, 2021, **129**, 107050.
59 T. Wu, Y. Chen, S. Shi, M. Wu, W. Gui, Y. Tan, J. Li and Y. Wu, *Materials*, 2021, **14**, 5450.
60 Z. Jia, T. Yang, L. Sun, Y. Zhao, W. Li, J. Luan, F. Lyu, L.-C. Zhang, J. J. Kruzic, J.-J. Kai, J. C. Huang, J. Lu and C. T. Liu, *Adv. Mater.*, 2020, **32**, 2000385.
61 B. Schuh, F. Mendez-Martin, B. Völker, E. P. George, H. Clemens, R. Pippan and A. Hohenwarter, *Acta Mater.*, 2015, **96**, 258–268.
62 Y. L. Zhao, T. Yang, Y. R. Li, L. Fan, B. Han, Z. B. Jiao, D. Chen, C. T. Liu and J. J. Kai, *Acta Mater.*, 2020, **188**, 517–527.
63 W. Guo, W. Dmowski, J.-Y. Noh, P. Rack, P. K. Liaw and T. Egami, *Metall. Mater. Trans. A*, 2013, **44**, 1994–1997.
64 W. Li, D. Wang, Y. Zhang, L. Tao, T. Wang, Y. Zou, Y. Wang, R. Chen and S. Wang, *Adv. Mater.*, 2020, **32**, 1907879.
65 R.-Q. Yao, Y.-T. Zhou, H. Shi, W.-B. Wan, Q.-H. Zhang, L. Gu, Y.-F. Zhu, Z. Wen, X.-Y. Lang and Q. Jiang, *Adv. Funct. Mater.*, 2021, **31**, 2009613.
66 M. Cui, C. Yang, B. Li, Q. Dong, M. Wu, S. Hwang, H. Xie, X. Wang, G. Wang and L. Hu, *Adv. Energy Mater.*, 2021, **11**, 2002887.
67 C. Zhan, Y. Xu, L. Bu, H. Zhu, Y. Feng, T. Yang, Y. Zhang, Z. Yang, B. Huang, Q. Shao and X. Huang, *Nat. Commun.*, 2021, **12**, 6261.
68 Z. Chen, J. Wen, C. Wang and X. Kang, *Small*, 2022, **18**, 2204255.
69 T. Yu, Y. Zhang, Y. Hu, K. Hu, X. Lin, G. Xie, X. Liu, K. M. Reddy, Y. Ito and H.-J. Qiu, *ACS Mater. Lett.*, 2022, **4**, 181–189.
70 H. Li, M. Sun, Y. Pan, J. Xiong, H. Du, Y. Yu, S. Feng, Z. Li, J. Lai, B. Huang and L. Wang, *Appl. Catal., B*, 2022, **312**, 121431.
71 D. Zhang, H. Zhao, X. Wu, Y. Deng, Z. Wang, Y. Han, H. Li, Y. Shi, X. Chen, S. Li, J. Lai, B. Huang and L. Wang, *Adv. Funct. Mater.*, 2021, **31**, 2006939.
72 D. Zhang, Y. Shi, H. Zhao, W. Qi, X. Chen, T. Zhan, S. Li, B. Yang, M. Sun, J. Lai, B. Huang and L. Wang, *J. Mater. Chem. A*, 2021, **9**, 889–893.
73 Y. Xin, S. Li, Y. Qian, W. Zhu, H. Yuan, P. Jiang, R. Guo and L. Wang, *ACS Catal.*, 2020, **10**, 11280–11306.
74 X. Wang, Q. Dong, H. Qiao, Z. Huang, M. T. Saray, G. Zhong, Z. Lin, M. Cui, A. Brozena, M. Hong, Q. Xia, J. Gao, G. Chen,

© 2023 The Author(s). Published by the Royal Society of Chemistry

Open Access Article. Published on 19 ottobre 2023. Downloaded on 01/06/2026 19:16:00.
This article is licensed under a Creative Commons Attribution-NonCommercial 3.0 Unported Licence.

R. Shahbazian-Yassar, D. Wang and L. Hu, *Adv. Mater.*, 2020, **32**, 2002853.
75 W. Shi, H. Liu, Z. Li, C. Li, J. Zhou, Y. Yuan, F. Jiang, K. Fu and Y. Yao, *SusMat*, 2022, **2**, 186–196.
76 C. Nataraj, E. J. L. Borda, A. van de Walle and A. Samanta, *Acta Mater.*, 2021, **220**, 117269.
77 X. Yang, S. Liping, L. Qiang, H. Lihua and Z. Hui, *J. Mater. Chem. A*, 2022, **10**, 17633–17641.
78 Q. Li, C. Jiang and Y. Du, *Mater. Technol.*, 2023, **38**, 2200660.
79 R. Jain, S. K. Dewangan, V. Kumar and S. Samal, *Mater. Sci. Eng., A*, 2020, **797**, 140059.
80 D. Wang, Z. Chen, Y. Wu, Y.-C. Huang, L. Tao, J. Chen, C.-L. Dong, C. V. Singh and S. Wang, *Smartmat*, 2023, **4**, e1117.
81 I. N. Yakovkin and N. V. Petrova, *Comput. Mater. Sci.*, 2023, **228**, 112356.
82 M. R. Zamani, M. Roostaei, H. Mirzadeh, M. Malekan and M. Song, *Curr. Opin. Solid State Mater. Sci.*, 2023, **27**, 101105.
83 X. Liu, J. Zhang and Z. Pei, *Prog. Mater. Sci.*, 2023, **131**, 101018.
84 S. Hou, M. Sun, M. Bai, D. Lin, Y. Li and W. Liu, *Acta Mater.*, 2022, **228**, 117742.
85 X. Liu, Y. Zhu, C. Wang, K. Han, L. Zhao, S. Liang, M. Huang and Z. Li, *J. Alloys Compd.*, 2023, **966**, 171547.
86 T. A. A. Batchelor, J. K. Pedersen, S. H. Winther, I. E. Castelli, K. W. Jacobsen and J. Rossmeisl, *Joule*, 2019, **3**, 834–845.
87 A. J. Medford, A. Vojvodic, J. S. Hummelshøj, J. Voss, F. Abild-Pedersen, F. Studt, T. Bligaard, A. Nilsson and J. K. Nørskov, *J. Catal.*, 2015, **328**, 36–42.
88 D. Zhang, Y. Wang, Y. Peng, Y. Luo, T. Liu, W. He, F. Chen and M. Ding, *Adv Powder Technol.*, 2023, **2**, 100129.
89 Y. Mao, J. Chen, H. Wang and P. Hu, *Chin. J. Catal.*, 2015, **36**, 1596–1605.
90 T. Tang, Z. Wang and J. Guan, *Chin. J. Catal.*, 2022, **43**, 636–678.
91 X. Fu, J. Zhang, S. Zhan, F. Xia, C. Wang, D. Ma, Q. Yue, J. Wu and Y. Kang, *ACS Catal.*, 2022, **12**, 11955–11959.
92 M. Wei, Y. Sun, F. Ai, S. Xi, J. Zhang and J. Wang, *Appl. Catal., B*, 2023, **334**, 122814.
93 D. Kim, S. Surendran, Y. Jeong, Y. Lim, S. Im, S. Park, J. Y. Kim, S. Kim, T.-H. Kim, B. Koo, K. Jin and U. Sim, *Adv. Mater. Technol.*, 2022, 2200882.
94 Q. Mao, X. Mu, K. Deng, H. Yu, Z. Wang, Y. Xu, X. Li, L. Wang and H. Wang, *Adv. Funct. Mater.*, 2023, 2304963.
95 S. Trasatti, *J. Electroanal. Chem. Interfacial Electrochem.*, 1972, **39**, 163–184.
96 S.-Q. Chang, C.-C. Cheng, P.-Y. Cheng, C.-L. Huang and S.-Y. Lu, *Chem. Eng. J.*, 2022, **446**, 137452.
97 Q. Chen, X. Han, Z. Xu, Q. Chen, Q. Wu, T. Zheng, P. Wang, Z. Wang, J. Wang, H. Li, Z. Xia and J. Hao, *Nano Energy*, 2023, **110**, 108380.
98 T. Tang, S. Li, J. Sun, Z. Wang and J. Guan, *Nano Res.*, 2022, **15**, 8714–8750.
99 X. Bai, L. Wang, B. Nan, T. Tang, X. Niu and J. Guan, *Nano Res.*, 2022, **15**, 6019–6025.
100 Y. Yu, H. Li, J. Liu, W. Xu, D. Zhang, J. Xiong, B. Li, A. O. Omelchuk, J. Lai and L. Wang, *J. Mater. Chem. A*, 2022, **10**, 21260–21265.
101 J. Yan, J. Zhu, D. Chen, S. Liu, X. Zhang, S. Yu, Z. Zeng, L. Jiang and F. Du, *J. Mater. Chem. A*, 2022, **10**, 9419–9426.
102 Y. Wen, P. Chen, L. Wang, S. Li, Z. Wang, J. Abed, X. Mao, Y. Min, C. T. Dinh, P. D. Luna, R. Huang, L. Zhang, L. Wang, L. Wang, R. J. Nielsen, H. Li, T. Zhuang, C. Ke, O. Voznyy, Y. Hu, Y. Li, W. A. Goddard Iii, B. Zhang, H. Peng and E. H. Sargent, *J. Am. Chem. Soc.*, 2021, **143**, 6482–6490.
103 A. Abdelhafiz, B. Wang, A. R. Harutyunyan and J. Li, *Adv. Energy Mater.*, 2022, **12**, 2200742.
104 R. He, L. Yang, Y. Zhang, X. Wang, S. Lee, T. Zhang, L. Li, Z. Liang, J. Chen, J. Li, A. Ostovari Moghaddam, J. Llorca, M. Ibáñez, J. Arbiol, Y. Xu and A. Cabot, *Energy Storage Mater.*, 2023, **58**, 287–298.
105 Z. Hou, C. Cui, Y. Li, Y. Gao, D. Zhu, Y. Gu, G. Pan, Y. Zhu and T. Zhang, *Adv. Mater.*, 2023, **35**, 2209876.
106 T. Zhang, G. Li, J. Liang, Z. Wen, W. Zhang, P.-q. Hou, S. Dong and Y. Qu, *J. Alloys Compd.*, 2023, **945**, 169319.
107 Y. Yao, Z. Li, Y. Dou, T. Jiang, J. Zou, S. Y. Lim, P. Norby, E. Stamate, J. O. Jensen and W. Zhang, *Dalton Trans.*, 2023, **52**, 4142–4151.
108 A. Holewinski and S. Linic, *J. Electrochem. Soc.*, 2012, **159**, H864–H870.
109 Z. Zhao, C. Chen, Z. Liu, J. Huang, M. Wu, H. Liu, Y. Li and Y. Huang, *Adv. Mater.*, 2019, **31**, 1808115.
110 Z. Lin, B. Ma, Z. Chen and Y. Zhou, *Ceram. Int.*, 2023, **49**, 23057–23067.
111 L. Jiang, Q. Yang, Z. Xia, X. Yu, M. Zhao, Q. Shi and Q. Yu, *RSC Adv.*, 2023, **13**, 5833–5850.
112 T. Tang, Z. Wang and J. Guan, *Adv. Funct. Mater.*, 2022, **32**, 2111504.
113 G. Wang, J. Chen, Y. Ding, P. Cai, L. Yi, Y. Li, C. Tu, Y. Hou, Z. Wen and L. Dai, *Chem. Soc. Rev.*, 2021, **50**, 4993–5061.
114 J. Cavin, A. Ahmadiparidari, L. Majidi, A. S. Thind, S. N. Misal, A. Prajapati, Z. Hemmat, S. Rastegar, A. Beukelman, M. R. Singh, K. A. Unocic, A. Salehi-Khojin and R. Mishra, *Adv. Mater.*, 2021, **33**, 2100347.
115 G. M. Tomboc, S. Choi, T. Kwon, Y. J. Hwang and K. Lee, *Adv. Mater.*, 2020, **32**, 1908398.
116 H. Li, J. Lai, Z. Li and L. Wang, *Adv. Funct. Mater.*, 2021, **31**, 2106715.
117 Y. Zhu, X. Cui, H. Liu, Z. Guo, Y. Dang, Z. Fan, Z. Zhang and W. Hu, *Nano Res.*, 2021, **14**, 4471–4486.
118 C. Zhan, L. Bu, H. Sun, X. Huang, Z. Zhu, T. Yang, H. Ma, L. Li, Y. Wang, H. Geng, W. Wang, H. Zhu, C.-W. Pao, Q. Shao, Z. Yang, W. Liu, Z. Xie and X. Huang, *Angew. Chem., Int. Ed.*, 2023, **62**, e202213783.
119 W. Chen, S. Luo, M. Sun, X. Wu, Y. Zhou, Y. Liao, M. Tang, X. Fan, B. Huang and Z. Quan, *Adv. Mater.*, 2022, **34**, 2206276.
120 X. Zuo, R. Yan, L. Zhao, Y. Long, L. Shi, Q. Cheng, D. Liu and C. Hu, *J. Mater. Chem. A*, 2022, **10**, 14857–14865.

© 2023 The Author(s). Published by the Royal Society of Chemistry

Open Access Article. Published on 19 ottobre 2023. Downloaded on 01/06/2026 19:16:00.
This article is licensed under a Creative Commons Attribution-NonCommercial 3.0 Unported Licence.

121 D. Liu, M. Chen, X. Du, H. Ai, K. H. Lo, S. Wang, S. Chen, G. Xing, X. Wang and H. Pan, *Adv. Funct. Mater.*, 2021, **31**, 2008983.
122 T. Zhang, J. Sun and J. Guan, *Nano Res.*, 2023, **16**, 8684–8711.
123 L. Xiao, J. Han, Z. Wang and J. Guan, *Int. J. Hydrogen Energy*, 2023, **48**, 23776–23784.
124 D. Roy, S. C. Mandal and B. Pathak, *J. Phys. Chem. Lett.*, 2022, **13**, 5991–6002.
125 Y. Wang, N. Gong, H. Liu, W. Ma, K. Hippalgaonkar, Z. Liu and Y. Huang, *Adv. Mater.*, 2023, **35**, 2302067.
126 Y. Lu, K. Huang, X. Cao, L. Zhang, T. Wang, D. Peng, B. Zhang, Z. Liu, J. Wu, Y. Zhang, C. Chen and Y. Huang, *Adv. Funct. Mater.*, 2022, **32**, 2110645.
127 G. Yang, Y. Zhao, D.-H. Lee, J.-M. Park, M.-Y. Seok, J.-Y. Suh, U. Ramamurty and J.-i. Jang, *Scr. Mater.*, 2019, **161**, 23–27.
128 C. Xie, D. Yan, H. Li, S. Du, W. Chen, Y. Wang, Y. Zou, R. Chen and S. Wang, *ACS Catal.*, 2020, **10**, 11082–11098.
129 P. Yang, Z. Jiang, Y. Shi, X. Ren, L. Liang, Q. Shao and K. Zhu, *J. Alloys Compd.*, 2023, **947**, 169699.
130 S. Dou, L. Tao, R. Wang, S. El Hankari, R. Chen and S. Wang, *Adv. Mater.*, 2018, **30**, 1705850.
131 D. Wang, Y. Zou, L. Tao, Y. Zhang, Z. Liu, S. Du, S. Zang and S. Wang, *Chin. Chem. Lett.*, 2019, **30**, 826–838.
132 Y. Sun and K. Liu, *J. Appl. Phys.*, 2018, **125**, 082402.
133 T. Wu, M. Sun and B. Huang, *Small*, 2020, **16**, 2002434.
134 M. Luo and S. Guo, *Nat. Rev. Mater.*, 2017, **2**, 17059.
135 D. Wang, Z. Chen, Y.-C. Huang, W. Li, J. Wang, Z. Lu, K. Gu, T. Wang, Y. Wu, C. Chen, Y. Zhang, X. Huang, L. Tao, C.-L. Dong, J. Chen, C. V. Singh and S. Wang, *Sci. China Mater.*, 2021, **64**, 2454–2466.
136 T. Löffler, A. Savan, H. Meyer, M. Meischein, V. Strotkötter, A. Ludwig and W. Schuhmann, *Angew. Chem., Int. Ed.*, 2020, **59**, 5844–5850.
137 L. Liu, H. Akhoundzadeh, M. Li and H. Huang, *Small Methods*, 2023, **7**, 2300482.
138 C. Wu, M. Jin, D. Guo, L. Wu, C. Wang, X. a. Chen and S. Wang, *Adv. Sustainable Syst.*, 2023, 2300192.

© 2023 The Author(s). Published by the Royal Society of Chemistry